NAVAL POSTGRADUATE SCHOOL
Monterey, California

THESIS

MULTI-FRACTAL ANALYSIS OF NOCTURNAL BOUNDARY
LAYER TIME SERIES FROM THE BOULDER
ATMOSPHERIC OBSERVATORY

by

Alex Joseph DeCaria

March 1992

Thesis Advisor: Ray Kamada

Approved for public release; distribution is unlimited

REPORT DOCUMENTATION PAGE

Form Approved
OMB No 0704-0188

1a REPORT SECURITY CLASSIFICATION UNCLASSIFIED	1b RESTRICTIVE MARKINGS
2a. SECURITY CLASSIFICATION AUTHORITY	3 DISTRIBUTION/AVAILABILITY OF REPORT Approved for public release; distribution is unlimited.
2b. DECLASSIFICATION/DOWNGRADING SCHEDULE	
4 PERFORMING ORGANIZATION REPORT NUMBER(S)	5 MONITORING ORGANIZATION REPORT NUMBER(S)

6a NAME OF PERFORMING ORGANIZATION Naval Postgraduate School	6b. OFFICE SYMBOL (If applicable) 35	7a NAME OF MONITORING ORGANIZATION Naval Postgraduate School
6c. ADDRESS (City, State, and ZIP Code) Monterey, CA 93943-5000		7b ADDRESS (City, State, and ZIP Code) Monterey, CA 93943-5000

8a. NAME OF FUNDING/SPONSORING ORGANIZATION	8b OFFICE SYMBOL (If applicable)	9 PROCUREMENT INSTRUMENT IDENTIFICATION NUMBER

8c. ADDRESS (City, State, and ZIP Code)	10 SOURCE OF FUNDING NUMBERS			
	PROGRAM ELEMENT NO	PROJECT NO	TASK NO	WORK UNIT ACCESSION NO

11. TITLE (Include Security Classification) MULTI-FRACTAL ANALYSIS OF NOCTURNAL BOUNDARY LAYER TIME SERIES FROM THE BOULDER ATMOSPHERIC OBSERVATORY

12 PERSONAL AUTHOR(S) DeCaria, Alex J.

13a. TYPE OF REPORT Master's Thesis	13b TIME COVERED FROM _____ TO _____	14 DATE OF REPORT (Year, Month, Day) March 1992	15 PAGE COUNT 59

16 SUPPLEMENTARY NOTATION The views expressed in this thesis are those of the author and do not reflect the official policy or position of the Department of Defense or the U. S. Government

17 COSATI CODES			18 SUBJECT TERMS (Continue on reverse if necessary and identify by block number) Fractals, Gravity Waves, Turbulence, Boundary Layer Meteorology, Time Series.
FIELD	GROUP	SUB-GROUP	

19 ABSTRACT (Continue on reverse if necessary and identify by block number)

Time series from a nocturnal boundary layer are analyzed using fractal techniques. The behavior of the self-affine fractal dimension, D_A, is found to drop during a gravity wave train and rise with turbulence. D_A is proposed as a time series conditional sampling criterion for distinguishing waves from turbulence. Only weak correlations are found between D_A and bulk turbulence measures such as Brunt-Vaisala frequency, Richardson number, and buoyancy length. The advantages of D_A analysis over turbulent kinetic energy (TKE), its component variances, FFT spectra, and self-similar fractals are also discussed in terms of local versus global basis functions, dimensional suitability, noise, algorithm complexity, and other factors. D_A was found to be the only measure capable of reliably distinguishing the wave from turbulence.

20. DISTRIBUTION/AVAILABILITY OF ABSTRACT ☒ UNCLASSIFIED/UNLIMITED ☐ SAME AS RPT ☐ DTIC USERS	21 ABSTRACT SECURITY CLASSIFICATION UNCLASSIFIED
22a NAME OF RESPONSIBLE INDIVIDUAL Ray Kamada	22b TELEPHONE (Include Area Code) (408) 646-2674 — 22c OFFICE SYMBOL PHKD

DD Form 1473, JUN 86 — Previous editions are obsolete. — SECURITY CLASSIFICATION OF THIS PAGE

S/N 0102-LF-014-6603

Approved for public release; distribution is unlimited.

Multi-fractal Analysis of Nocturnal Boundary Layer Time Series
from the Boulder Atmospheric Observatory

by

Alex Joseph DeCaria
Lieutenant, United States Navy
B.S., University of Utah, 1985

Submitted in partial fulfillment of the
requirements for the degree of

MASTER OF SCIENCE IN METEOROLOGY AND PHYSICAL OCEANOGRAPHY

from the

NAVAL POSTGRADUATE SCHOOL
March, 1992

ABSTRACT

Time series from a nocturnal boundary layer are analyzed using fractal techniques. The behavior of the self-affine fractal dimension, D_A, is found to drop during a gravity wave train and rise with turbulence. D_A is proposed as a time series conditional sampling criterion for distinguishing waves from turbulence. Only weak correlations are found between D_A and bulk turbulence measures such as Brunt-Väisälä frequency, Richardson number, and buoyancy length. The advantages of D_A analysis over turbulent kinetic energy (TKE), its component variances, FFT spectra, and self-similar fractals are also discussed in terms of local versus global basis functions, dimensional suitability, noise, algorithmic complexity, and other factors. D_A was found to be the only measure capable of reliably distinguishing the wave from turbulence.

TABLE OF CONTENTS

I. INTRODUCTION

A. PROBLEM STATEMENT.

It is important to separate turbulence from gravity waves in the atmospheric boundary layer, whether in studying wave/turbulence interaction, or in modeling the dispersion of passive scalars such as pollutants and aerosols. This is because turbulence and gravity waves differ greatly in phase coherence, periodicity, and transport properties. Also, purely linear waves transport only momentum and energy, while both non-linear waves and turbulence can transport heat and scalars (Stull, 1988). However, turbulent transport greatly exceeds that of non-linear waves. Thus, using temperature, pressure, or wind speed variances can lead to dispersion overestimates, if gravity waves and turbulence are both present. Vertical humidity transport also depends on the presence of gravity waves; this affects stratus cloud and radiation fog formation. However, current methods of separating waves from turbulence either do not apply to a broad spectrum of cases, or are not operationally useful.

B. THE GOAL.

The goal is to see if the fractal dimension of a temperature or wind speed time series can be used to distinguish atmospheric boundary layer waves from turbulence. A related goal is to compare the relative merits of fractal dimension and other, more standard wave/turbulence measures such as Richardson number (R_i), Brunt-Väisälä frequency (BVF), buoyancy length scale (l_B), Fourier spectra, variances, and turbulent kinetic energy (TKE), applied to wave/turbulence discrimination.

C. WHY FRACTALS?

Real turbulence and waves should display quite different values of fractal dimension because pure waves are not self-similar. Thus fractal

1

dimension may be a useful wave/turbulence discriminator. The following discusses this possibility in more detail.

1.   **Fractals and Turbulence.**

Fractal geometry is part of the chaos and non-linear dynamical systems theory, developed over the past few decades (Moon, 1987). Fractal geometry appears ideally suited for studying turbulent flows in the atmosphere because it is based on self-similarity. Self-similarity is defined as, "A property of a set of points in which geometric structure on one length scale is similar to that at another length scale." (Moon, ibid) In fluids where waves or eddies lack rigid geometric structure, it implies that the statistical properties describing the ensemble mean geometry of the flow structure at one scale are similar to those at a different scale. Richardson (1922) recognized this self-similarity when he wrote,

"Bigger whorls have little whorls,
    which feed on their velocity,
  and little whorls have lesser whorls,
    and so on to viscosity."

Sreenivasan and Meneveau (1986), and Presad and Sreenivasan (1990) established that interfacial convolutions between turbulent and non-turbulent regions of a shear flow are self-similar and therefore have a fractal dimension. Schertzer and Lovejoy (1984) used the concept of self-affine fractals to show that no abrupt transition from two to three dimensional turbulence exists between large and small atmospheric eddies; rather, atmospheric stability induces a dimensional continuum from synoptic to Kolmogorov scales. Self-affinity is a generalization of self-similarity, discussed extensively in Chapters II and III.

2.   **Fractal Dimension _of_ vs. _from_ a Time Series.**

Packard et al. (1980) and Pawelzik and Schuster (1987) have studied fractal dimensions of chaotic systems inferred from a time series. These authors studied the dimension of the attractor of the chaotic system. Moon (ibid) defines an attractor as, "A set of points or a

subspace in phase space toward which a time history approaches after transients die out."

The aim here is to find the fractal dimension of the time series itself, not the dimension of the phase space attractor or the dimension of the turbulence field in real space.

Since a time series is a digital sampling, a time series trace of a fractal process should also show fractal characteristics. For example, Carter et al. (1986) found that the known fractal characteristics of cloud geometry in real space were also evident in an apparent time series of their infrared intensity versus azimuth viewing angle.

3.   **Advantages of Fractal Analysis.**

Fractal analysis has potential advantages over standard spectral analyses.   1)   Less data manipulation is required.   Standard Fourier transform techniques require that the data be periodic within the data window to avoid introducing high frequency noise into the spectrum.   This requires tapering the data within the window so that its endpoints have the same value.   2)   Fractal analysis' biggest advantage is that data breaks, such as truncated gravity wave trains or breaking Kelvin-Helmholtz instabilities and other such discontinuities pose no problems.   In Fourier analyses a linear combination of wave numbers much higher than the time resolution is required to accurately account for such break points.   This is because the basis functions for standard spectral analysis: sinusoids, Legendre or Leguerre polynomials, Bessel functions, etc., are infinite in length, rather than discrete; whereas in fractal analysis, the resolution itself becomes a discrete Chapeau basis function.   And this basis function inherently spans the ideal range: from the chosen span of the time series to the available limit of resolution.   Chapeau functions shorter than the available resolution are not required to portray discontinuities.

The above does not imply that fractal analysis should replace traditional spectral analysis.   But fractal analysis may supplement and

sometimes substitute for Fourier and other standard techniques, particularly in discriminating waves from turbulence in a time series.

II. THEORY

A. CURRENT METHODS OF SEPARATING WAVES FROM TURBULENCE.

Some current methods of separating waves from turbulence are discussed as follows.

1. Cross-spectral Method.

Described in Finnigan (1988), this method assumes, since linear waves do not transport heat, that for waves the vertical velocity cross spectrum with temperature exhibits a small cospectrum and large quadrature spectrum, but for turbulence a large cospectrum and small quadrature spectrum (i.e., the temperature wave lags the vertical velocity wave by 90° in phase). Though this sounds appealing, Finnigan reports that, "...linear behavior of gravity waves close to the ground is the exception rather than the rule so that the condition of the quadrature spectrum [being] much greater than the cospectrum is of no value as a wave detector."

2. Spectral Gap Method.

Nai-Ping (1983) lists several authors who find a wave/turbulence gap in the boundary layer power spectra. Caughey (1977) relates the position of the spectral gap to the Brunt-Väisälä frequency (BVF), which theoretically is the highest frequency of gravity wave that the atmosphere will support. The method is unreliable since spectral gaps are not guaranteed. Finnigan (ibid) states further that, "A characteristic of gravity waves that interact strongly with turbulence is that, while their wavelengths are much longer than any turbulent length scale, their frequencies are within the energy-containing range of the turbulence." That is, though turbulence and waves may both be advected by mean winds, waves have an additional phase velocity which is included in their apparent frequency with respect to a fixed sensor. Thus, a spectral gap may exist in wave number, but not in the frequency domain which must be

5

used to separate waves from turbulence in a time series. Caughey and Readings (1975) concur, saying, "In the presence of significant turbulence, however, it is difficult to see how even these [spectral] techniques will help unless the wave and turbulence fall in different frequency bands."

      3.   **Phase Averaging.**

Finnigan (ibid) describes this method as "...taking ensemble averages of the time series, the ensembles being consecutive portions of the record with the duration of each portion equal to the period of a chosen reference wave."

Phase averaging identifies a single wave portion of the signal, and for example, is used operationally to separate ocean tide constituents. Subtracting the wave and mean from the signal leaves turbulence as the remainder. One drawback is that the wave frequencies must be known *a priori*. This presents no difficulty when dealing with ocean tides, since the frequencies are well known. But for the atmosphere, gravity wave frequency is not always known. The most reliable evidence of near surface gravity waves is periodic surface pressure fluctuations (Finnigan, ibid); thus, a surface microbarograph array or more complex methods are needed to determine wave frequency. However, most tower sites lack microbarographs. Further complications arise for phase averaging if wave amplitudes change greatly with time, if the wave loses coherence after a few periods, or if dispersion changes the wave frequency. However, the discussion below shows how fractal analysis avoids many of these difficulties.

B.   BASIC CONCEPTS OF SELF-SIMILAR FRACTAL DIMENSION.

The minimum number of boxes of side ε (or circles of diameter ε) needed to cover a set of points on a two-dimensional plot scales as

$$N(\varepsilon) \approx \frac{F}{\varepsilon^D} \ , \qquad\qquad (II.1)$$

where D is defined as the capacity dimension of the set (Moon, ibid), and F is the lacunity (see Section C). If the set consists of a straight line, then D = 1 because twice as many boxes are needed to cover the line if the box length is cut in half. If the set consists of uniformly distributed points in a plane, then D = 2, since four times as many boxes are needed to cover this set if the box length is halved.

If the points are not uniformly distributed, then D can be non-integer. The set of points is then fractal, and the sets' fractal dimension is given as D, defined in the limit as ε approaches zero. This definition is called the box dimension, D_B, (Mandelbrot, 1985), and is given as

$$D_B = \lim_{\varepsilon \to 0} \frac{\log N(\varepsilon)}{\log \frac{1}{\varepsilon}} \ . \qquad\qquad (II.2)$$

The Cantor set, shown in Figure 1, is an example of a set having non-integer D_B. This set is formed from a line segment by removing its middle third. The middle third of each remaining segment is then removed, and the process is repeated to infinity. This set is self-similar because the geometric structure displayed at a length scale of unity is reproduced, or similar to all scales removed by successive factors of three. If the original line length is unity, N(1)=1 boxes of side ε = 1 are needed to cover the set. If $\varepsilon=1/3$ then N(1/3)=2, and if $\varepsilon=1/9$, then N(1/9)=4, etc. Thus, ε is generally 3^n, and $N(\varepsilon)$ is 2^n, where n = 0,1,2,3,...,∞ (Grebogi et al., 1987).

From equation II.2, noting that n$\to\infty$ implies $\varepsilon\to0$, D_B for the Cantor set becomes
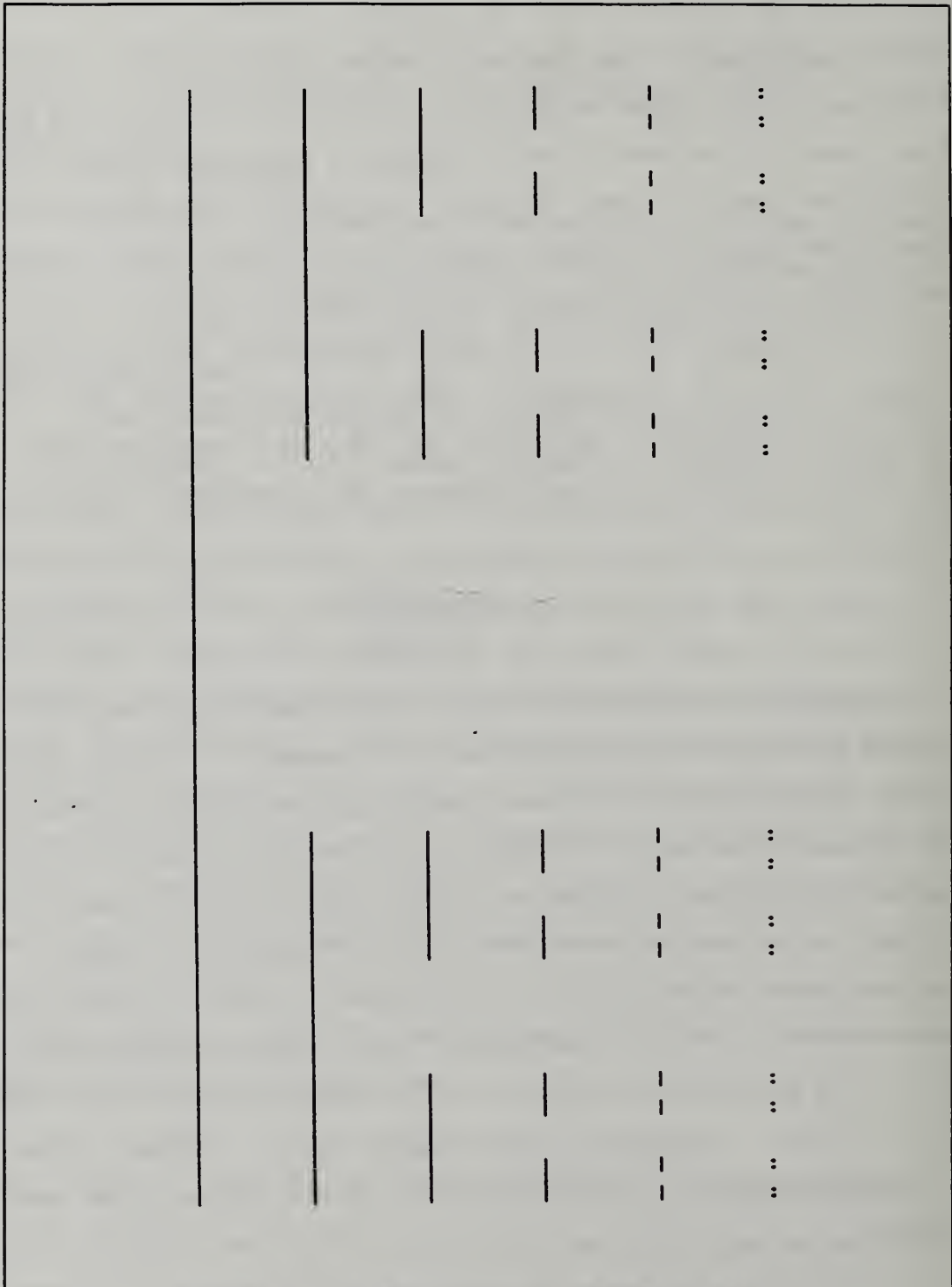
Figure 1 - Construction of the Cantor set.

$$D_B = \lim_{n \to \infty} \frac{\log 2^n}{\log 3^n} = \frac{\log 2}{\log 3} = 0.63092\ldots \qquad (II.3)$$

intermediate between a point ($D_B = 0$) and a line ($D_B = 1$).

Unlike the analytic Cantor set, D_B must be evaluated numerically for most fractal data sets. This is done by removing the limit in II.2 and reordering terms to get

$$\log N(\varepsilon) = \log F - D_B \log \varepsilon \; . \qquad (II.4)$$

Then $-D_B$ is the slope of the plot of log N(ε) vs. log ε, and log F is the y-intercept.

C.   ALTERNATIVE ALGORITHM FOR CALCULATING FRACTAL DIMENSION.

If a set of points, such as a geographical coastline, consists of a continuous curve in two dimensions, Mandelbrot (1977) describes another approach to determine fractal dimension. Here, curve length is defined as

$$L(\varepsilon) \approx \varepsilon \, N(\varepsilon) \; , \qquad (II.5)$$

where N(ε) is given as

$$N(\varepsilon) = \frac{F}{\varepsilon^D} \; , \qquad (II.6)$$

and F is again the lacunity.

Lacunity relates the "length" of one fractally scaling curve to another of the same D. To illustrate, assume that the eastern coastline of the United States is fractal, and C is constant along its entire length. The D from Baltimore to Norfolk is the same as from Baltimore to Miami. For any ε, segment two will clearly be longer in measure than segment one. Then, II.6 show that the step length ratio will be

Using II.6 in II.5, L(ε) can be written as

$$\frac{N_1(\varepsilon)}{N_2(\varepsilon)} = \frac{\dfrac{F_1}{\varepsilon^D}}{\dfrac{F_2}{\varepsilon^D}} = \frac{F_1}{F_2} \ . \tag{II.7}$$

$$L(\varepsilon) \approx F\varepsilon^{1-D} \ . \tag{II.8}$$

Taking the log of II.8 yields the straight line equation,

$$\log L(\varepsilon) = \log F + (1-D)\log \varepsilon \ . \tag{II.9}$$

Plotting log $L(\varepsilon)$ versus log ε, the resulting slope yields $(1 - D)$. To find D, first find $L(\varepsilon)$ at the maximum value of ε, ε_o. Then, from II.9, log $L(\varepsilon_o) = \log F + (1-D)\log\varepsilon_o$. Now find $L(\varepsilon)$ at the smallest available ε, ε_i, so II.9 becomes log $L(\varepsilon_i) = \log F + (1-D)\log \varepsilon_i$. This yields two equations with two unknowns, D and F, so ideally,

$$D = \frac{\log\left[\dfrac{L(\varepsilon_o)}{L(\varepsilon_i)}\right]}{\log\left[\dfrac{\varepsilon_o}{\varepsilon_i}\right]} \ . \tag{II.10}$$

In practice, the measured time series will contain some noise, so $L(\varepsilon)$ will not be exact. Also, the data may only be fractal over a certain range, so that the choice of ε_o and ε_i is not completely objective. Thus, multiple values of $L(\varepsilon)$ should be found, and some form of regression used to find the slope of the log-log plot. This is discussed further in Chapter III.

This algorithm is equivalent to covering the curve with circles of diameter ε, so that $L(\varepsilon)$ is the minimum number of circles of diameter ε required to cover the curve times their diameter. Thus, $L(\varepsilon)$ is measured by opening a compass to a constant span, ε, and walking its legs along the curve.

Mandelbrot (1985) calls this estimate the "compass dimension", D_C. To show that D_C us equivalent to D_B, take II.8 and solve for D to get

$$D = \frac{\log L(\varepsilon) - \log(F)}{\log\frac{1}{\varepsilon}} + 1 \ . \qquad\qquad \text{(II.11)}$$

Substituting L(ε) from II.5 gives

$$D = \frac{\log N(\varepsilon) - \log(F)}{\log\frac{1}{\varepsilon}} \ , \qquad\qquad \text{(II.12)}$$

and in the limit as $\varepsilon \rightarrow 0$, since N($\varepsilon$) is much larger than F, this yields

$$D = \lim_{\varepsilon \to 0} \frac{\log N(\varepsilon)}{\log\frac{1}{\varepsilon}} \ , \qquad\qquad \text{(II.13)}$$

which is D_B.

Fractal geometry can be used to measure the jaggedness or degree of convolution of a curve. Mandelbrot (1977), and Sreenivasan and Meneveau (ibid) show that the length of a self-similar curve increases without limit as the resolution increases. This length increase follows a power law, and the fractal dimension of the curve can be inferred from the exponent. The fractal measure of curve jaggedness is central to this thesis.

D. D_C COMPARED WITH D_B.

Though D_C and D_B are identical, which is easier to calculate for a time series? A box algorithm divides the data plane into discrete boxes of length ε, where N(ε) gives the number of boxes containing at least one point of the curve. With digitized data the shape of the curve between discrete data points is unknown. Thus, it is simplest to assume a straight line Chapeau function between data points. As before, one plots log N(ε) vs logε to find D_B. ε cannot be smaller than the ordinate distance between three data points, $2\varepsilon_i$, because for $\varepsilon < \varepsilon_i$ the curve scales as a one dimensional line, the assumed shape between adjacent data points.

For the compass algorithm $L(\varepsilon) = \varepsilon N(\varepsilon)$. Then, the slope of the plot of $\log L(\varepsilon)$ vs $\log \varepsilon$ yields D_C.

Though both algorithms give identical results, the former is less efficient for a single curve. This is because every box in the domain must be checked, even though most boxes are empty, while compass stepping considers only filled circles with points on the curve. Thus, compass stepping is more efficient.

E.   APPLICATIONS TO TIME SERIES.

Several authors, Carter et al. (ibid), and McHardy and Czerny (1987), have measured fractal dimensions for time series. Unlike coastlines, a time series plot has axes with different units of measure. This poses a difficulty, for how can "length" of a time series trace be measured if the units are not uniquely defined? And once defined, will different scaling ratios give different values of D_C?

Mandelbrot (1985) shows that though calculable, D_C may be theoretically meaningless for a time series, and can actually exceed two if the y to x-axis scaling ratio is large enough. This requires a different approach to measuring fractal dimension, described in the next section.

F.   SELF AFFINE FRACTAL DIMENSION.

McHardy and Czerny (ibid) apply a slightly different, "self-affine", definition of fractal dimension when analyzing their time series data. "Self-similarity" implies that geometric structure or their ensemble statistical properties remain similar between scales removed along all axes by the same constant factor. "Self-affinity" requires at least one different constant factor among the axes. Thus, McHardy and Czerny define their self-affine "length metric" as

$$L(\varepsilon) \;=\; \frac{1}{\varepsilon} \int_{0}^{T} |F(t+\varepsilon) - F(t)| \, dt \;, \qquad\qquad (\text{II}.14)$$

where now the abscissa scaling changes by the same factor, $\varepsilon_n/\varepsilon_{n+1}$, each time that ε changes by the factor $\varepsilon_{n+1}/\varepsilon_n$ (their length metric differs from the more traditional self-affine length metric, which has the integrand, $([F(t+\varepsilon)-F(t)]^2 + \varepsilon^2)^{1\!/\!4}$. This leads to,

$$D \;=\; -\,\frac{d \log L(\varepsilon)}{d \log \varepsilon} \;. \qquad\qquad (\text{II}.15)$$

$L(\varepsilon)$ from II.14 will be much longer at small ε, but note that D in II.15 is defined as the rate of change of log length with log resolution, not the ratio of log length to log resolution. Since time, ε, cancels in the length metric, $L(\varepsilon)$ only has units of amplitude. This avoids arbitrary scalings between amplitude and time units and makes the problem one dimensional, so D is less than unity. II.14 seems the natural choice for evaluating time series. Hereafter, D from this method will be referred to as D_A.

G. D_A AND NOISE.

$L(\varepsilon)$ calculated from II.14 will contain some contribution from noise. The noise is statistically independent of the signal. If its level is known, its contribution to $L(\varepsilon)$ can be estimated by the formula, $L^2_{observed} = L^2_{signal} + L^2_{noise}$. White noise has $D_A = 1$, and its effect is to increase the fractal dimension of the time series. (McHardy and Czerny, ibid)

H. FRACTAL DIMENSION AND STABILITY.

To explain why D_A for an atmospheric time series might be related to stability, imagine three idealized cases:

      1. A very stable atmosphere with no perturbations,

      2. A stable atmosphere perturbed only by a single, linear gravity wave,

      3. An unstable, highly turbulent atmosphere.

In case 1, a time series of the velocity components, temperature, or pressure would be a straight line with a D_C of unity, or a D_A of zero.

A time series from case 2 would be a sinusoid with a frequency equal to that of the wave (Stull, ibid). D_C of a single sinusoid is in principle unity, and D_A zero, since it is not self-similar or self-affine. This is shown numerically by calculating D_A. Figure 2 shows the log $L(\varepsilon)$ versus log ε plot for this algorithm calculated on a sinusoid with a wavelength λ = 1800 units. The horizontal plateau through scales less than $\lambda/3$ shows that the wave looks one dimensional.

Since turbulence has been observed to be fractal (Sreenivasan and Meneveau, ibid), a time series from case 3 should be fractal, and have a dimension greater the previous cases.

If these three cases were the only ones possible, fractal dimension would clearly relate to stability, i.e., D_A would be zero for stable atmospheres and greater than zero for unstable atmospheres. The real atmosphere is a complex continuum of cases. For instance, a moderately stable atmosphere can still display intermittent turbulence, and thus have a D_A greater than zero.

The three simple cases illustrate that for a continuum of cases, fractal dimension will change with stability. However, they shed no detail on whether this change will be abrupt or smooth, what parameters will correlate with this change, or whether this change can be used to infer the presence, development, or decay of atmospheric gravity waves. This thesis investigates these issues.

I. RELEVANT CONCEPTS OF GRAVITY WAVE AND TURBULENCE THEORY.

1. Gravity Wave Characteristics.

Gravity waves in the stable boundary layer can be generated by a number of mechanisms, among them are wind shear (Kelvin-Helmholtz instability), impulses such as thunderstorms, and flow over an obstacle.
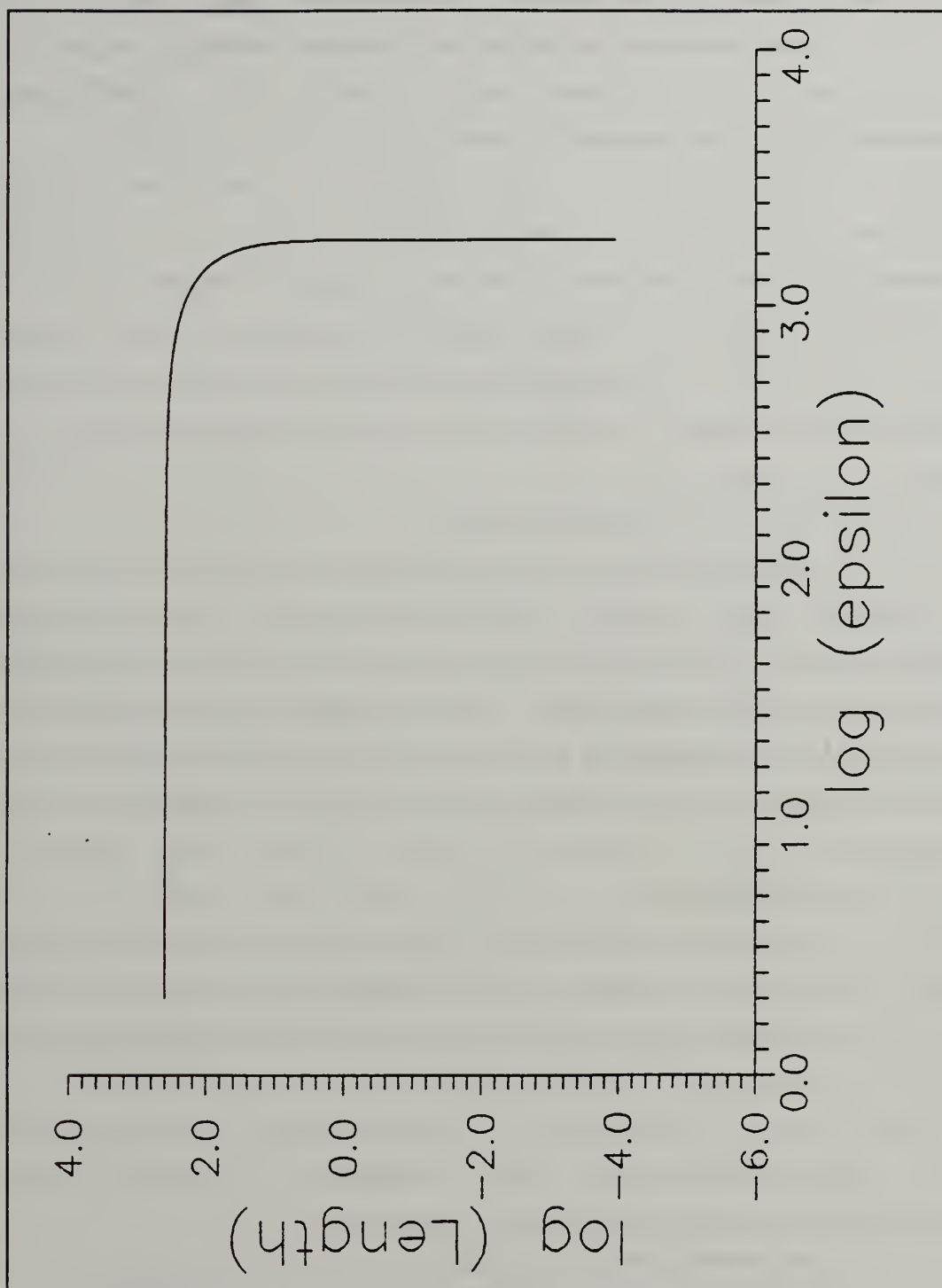
14

Figure 2 - Self-affine L(ε) for 1800 point sinusoid.

Their amplitudes can vary from a few centimeters to 200 meters, with wave periods of less than a minute up to 40 minutes (Stull, ibid).

The generation of waves by flow over an obstacle has particular significance in the present study. Hunt (1980) gives the natural wavelength of flow over a hill as

$$\lambda = 2\pi U_o/\text{BVF} ,\qquad\qquad (\text{II}.16)$$

where U_o is mean wind speed. The hill "length" is given as L_1, "...the distance from the hill top to where the elevation is half its maximum." He shows that if $\lambda \gtrsim 5L_1$ then lee waves are generated having λ much greater than the hill length. Further, Hunt shows that if $\lambda \lesssim 2L_1$ then strong lee waves are possible.

2. **Turbulence Characteristics.**

Unlike gravity waves, turbulence is treated stochastically due to finite computer power. It is seen as many different size eddies juxtaposed to and embedded within each other. Unlike gravity waves it is three dimensional, aperiodic, chaotic, quasi-random, and thus has been studied through statistics such as variances and covariances. Turbulence is also associated with either dynamic or static instability, with high Reynolds number, low Richardson number, and high fractal dimension.

3. **Transport.**

Linear waves differ from non-linear waves. Like turbulence, non-linear waves can transport energy, momentum, heat, and scalars such as aerosols, whereas purely linear waves transport only energy and momentum. This is because the temperature and vertical velocity fields of linear waves are exactly 90 degrees out of phase, so their covariance integrated over a wavelength is zero. So, it is important to distinguish waves from turbulence when predicting scalar dispersion.

4. **Turbulence and gravity waves.**

Many papers exist on gravity wave effects on turbulence generation and wave and turbulence interaction. The concept of a gravity

16

wave transferring energy to Kelvin-Helmholtz waves which then "break" is widely used as a model for turbulence generation by waves (Stull, ibid; Atlas et al., 1970), though this model is not universally accepted (Hines, 1988).

However, within this context, Gossard et al., (1985) suggests a generation mechanism for boundary layer turbulence where the local gradients of θ, u, and v increase steadily, together with decreasing turbulence. The vertical shear eventually reaches an insupportable value of local Richardson number, leading to local Kelvin-Helmholtz instability and a rapid onset of fluctuations growing into turbulence.

This mechanism will be discussed in the context of fractal observations in Chapter IV.

By phase averaging, Finnigan (ibid) was able to resolve the wave and turbulent portions of the total energy, and showed that, during the first quarter of a wave cycle, horizontal turbulent kinetic energy was generated. Vertical turbulence was generated during the subsequent third of the cycle. Both of these energies were transferred from the wave to the turbulence. They point out that the wave seemed to modulate the turbulence; however, the presence of the turbulence had no apparent effect on the wave.

The above cited papers, and many observational papers such as Caughey and Readings (ibid), Caughey (ibid), and Nai-Ping (ibid), make it apparent that waves and turbulence commonly coexist in the boundary layer, and turbulence generation can sometimes depend on the wave.

III. METHODS

A.   DATA.

The data sets used in this experiment were obtained from the Boulder Atmospheric Observatory (BAO), whose facilities are described by Kaimal and Gaynor (1983). The data consist of samples at eight different levels: 10, 22, 50, 100, 150, 200, 250, and 300 meters, of:

  1. u, v, and w velocity components sampled at 10 Hz by sonic anemometers.

  2. wind direction and speed at 1 Hz by propeller vane anemometers.

  3. temperature at 10 Hz by platinum wire thermometers, and at 1 Hz by quartz thermometers.

The 1 Hz data were available only as 10 second block averages. The 10 Hz data were available at both 10 Hz, and as 10 second block averages.

Noise levels for the data are $\leq$ .01 °C for the platinum wire thermometer, and $\leq$ .03 m s^{-1} for the sonic anemometers (personal communication with J. Gaynor, NOAA Wave Propagation Laboratory).

The data were provided on 9 track magnetic tapes. The tapes, and FORTRAN programs for reading them, were provided by John Gaynor and Dave Welch of the NOAA Wave Propagation Laboratory. These programs were run on a Sun 4 computer provided by the Naval Postgraduate School (NPS) Computer Science Department. The output from the programs was in unformatted, binary form. The data was analyzed on the NPS mainframe computer. Since the mainframe and Sun use different representations for binary numbers, the data files were converted to ASCII before electronic transfer to the mainframe.

18

The data covered three time periods. These periods are (in MST):

      Period A: 2340 September 7 through 0340 September 8, 1983

      Period B: 0440 through 0620 September 9, 1983

      Period C: 0000 through 0620 September 19, 1986

B.   PICKING A PERIOD OF INTEREST.

To pick a time period of interest, time series were plotted for the 10 Hz temperature data at levels 4 and 5 (100 and 150 meters) for all three time periods. Since the hope was to find gravity wave activity, the time series plots were checked visually for wave evidence. The temperature trace was inspected because it appeared to be the least noisy of the data available. Such a signature appeared during period A at level 4, between 0040 and 0105 MST, September 8, 1983. Figure 3 shows this time series, with the wave period occurring in windows 21 through 27.

The wave was believed to be induced by the southerly flow over a small hill to the south of the tower, since the prevailing winds were southerly throughout the time series. To investigate this, equation II.16 was used to calculate λ, with an observed BVF of 0.03 Hz, and U_o = 9 m s^{-1}. This yielded a value of $\lambda \approx 1900$ meters. The base of the hill was determined to be at an elevation of 5220 feet, and the top at 5280 feet. By the definition given in the previous chapter, L_l was measured horizontally from the top of the hill to the 5250 foot contour in the direction of the tower, a distance of around 250 meters; thus, $5L_l \approx 1250$ meters. This fits the condition for $\lambda \gtrsim 5L_l$ for lee waves to be generated by the hill.Both prior to and after the wave period, the BVF was less than 0.01 Hz. During these periods, λ would be greater than 6200 meters, which is well out of the range for lee wave formation. The appearance of the wave only when the condition for lee waves was met led to the conclusion that the observed wave was terrain induced. There were two other periods during windows 43 through 53, and 61 through 66, when conditions for wave generation were approached, but not as closely. Waves did not appear in
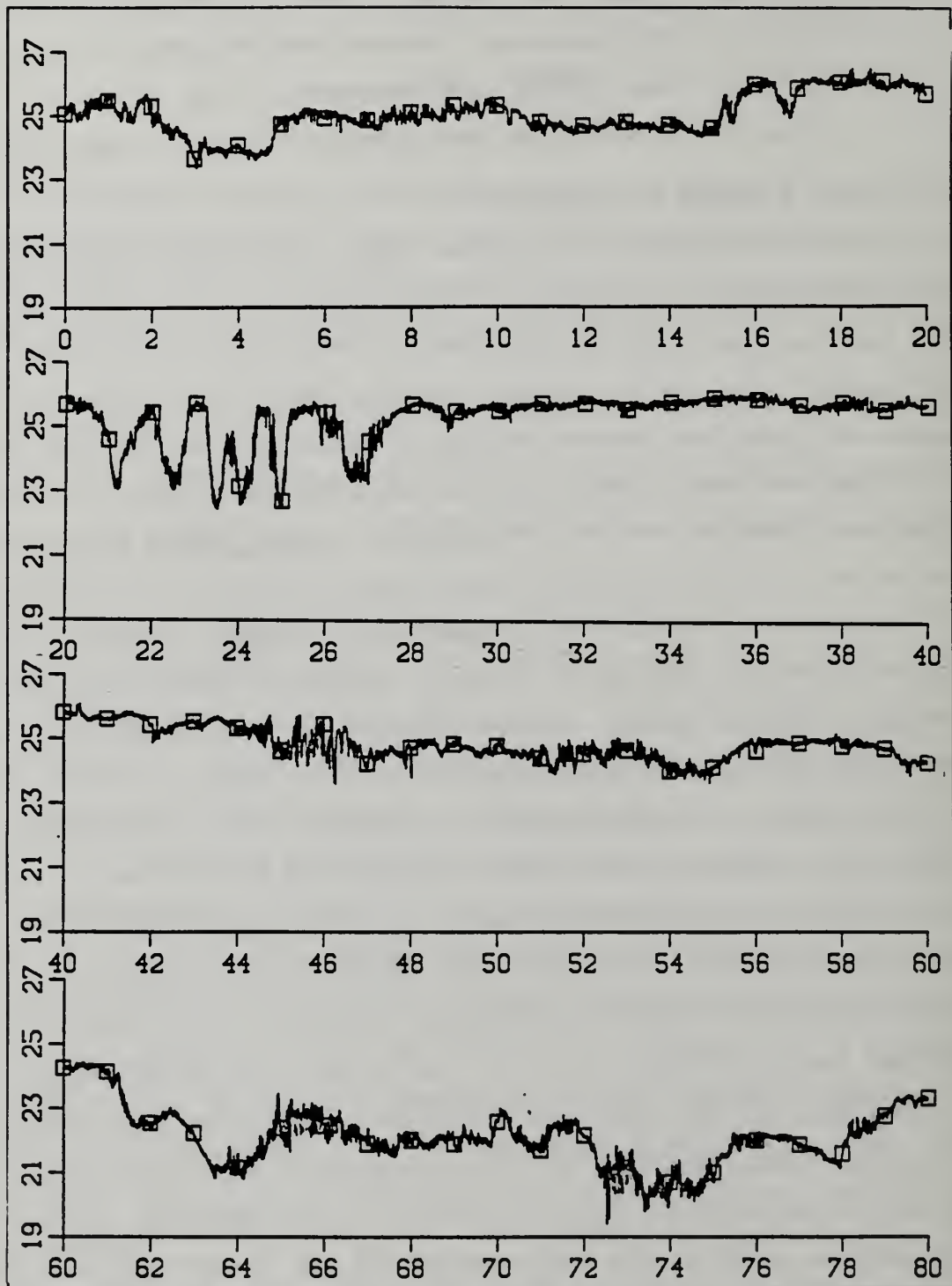
Figure 3 - Temperature (°C) vs. three minute windows. The wave occurs in windows 21 - 27; turbulence episodes in windows 45 - 47, 66 - 67, and 73 - 75.

the time series during these periods.

The other periods showed no clear evidence of waves. Period C showed pronounced noise spikes at 20 minute intervals, and high noise levels throughout most of its length.

Another feature of period A was a region of reduced temperature variance immediately following the "wave" episode. This allowed a comparison of the fractal characteristics of both wave and non-wave portions of the time series. Thus, the four hours from period A at level 4 was chosen for study.

C. ANALYSIS METHODS.

D_C, D_A, turbulent kinetic energy (TKE) and its component velocity variances, bulk Richardson number (R_B), Brunt-Väisälä frequency (BVF), buoyancy length (l_B), and fast fourier transform (FFT) spectra were all tested as analysis tools on the u, v, w, and T time series at level four. R_B, BVF, and l_B are bulk measures, and were taken across levels three to five, a vertical distance of 100 meters. The above parameters were checked for possible correlation with D_A.

The biggest disadvantage of bulk measures is that they are weighted over the entire layer, not at the sensor itself. D_C, D_A, TKE, FFT spectra, and variance are local values valid at the sensor only. Thus, if an eddy is smaller than 100 meters (the bulk layer thickness), then its effect will be measured locally at the sensor, and impact the local measures, but the eddy signature may not appear at levels above and below the level of interest where the gradients of U, V, and θ are measured. Thus, the eddy signature may appear on a local measure, but not on a bulk measure.

1. D_C analysis.

The characteristics of D_C of the time series were explored by applying Mandelbrot's "compass" algorithm to the data, and making log-log plots of the measured length of the time series versus ε. This was done for adjacent three minute long windows throughout the entire four hours of

21

the level 4, 10 Hz temperature data. The minimum ε on these plots was set to two data points (.2 sec), because for smaller ε the curve will scale linearly, due to the assumption of a straight line connecting the data points. The maximum ε was set equal to the size of the window, or 1800 data points, for the first run. For all runs, the coordinate axis of the time series was expanded by a factor of 100, so that .1 seconds on the ordinate was equal to .01°C on the coordinate.

The first run showed for all windows that the curve scaled linearly (the slope on the log-log plots was zero) for all log $\varepsilon \geq 2.25$, or $\varepsilon > 17.8$ seconds. For most windows, the linearly scaling portion began above $\varepsilon \geq 3.2$ seconds. To get better resolution on the fractal portion of the curve, the run was repeated with a maximum $\varepsilon = 178$. A typical plot from this run is shown in Figure 4.

To get D_C for a given window, a regression line must be fitted to the steeper, linear portion of the curve. The simple linear regression from Beyer (1987) was used for this process. The linear region varied from window to window, depending on the upper scale of what was presumed to be the turbulent eddies. The upper cut-off, ε_o, for the range used in the regression was determined manually for each window. To be most objective, the following algorithm was used:

1. A line was drawn with a straight edge along the steepest, linear portion of the curve (point A in Figure 5).

2. A second line was drawn with a straight edge along the shallow, trailing edge of the curve at high values of log ε.

3. The ordinate where these two lines intersected was taken as the upper cutoff.

Some windows also required that the minimum ε used for the regression, ε_i, be determined manually in a similar fashion.
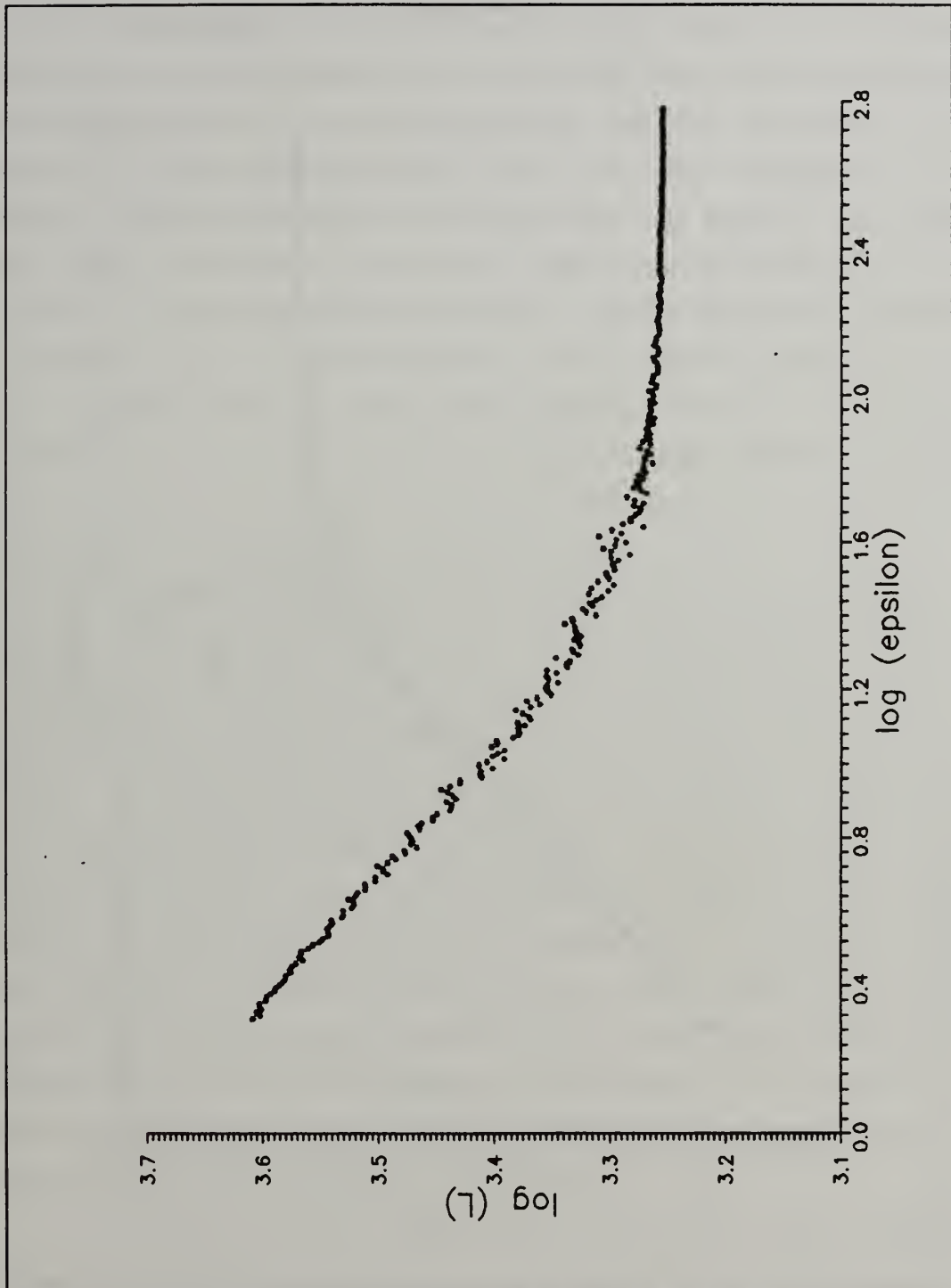
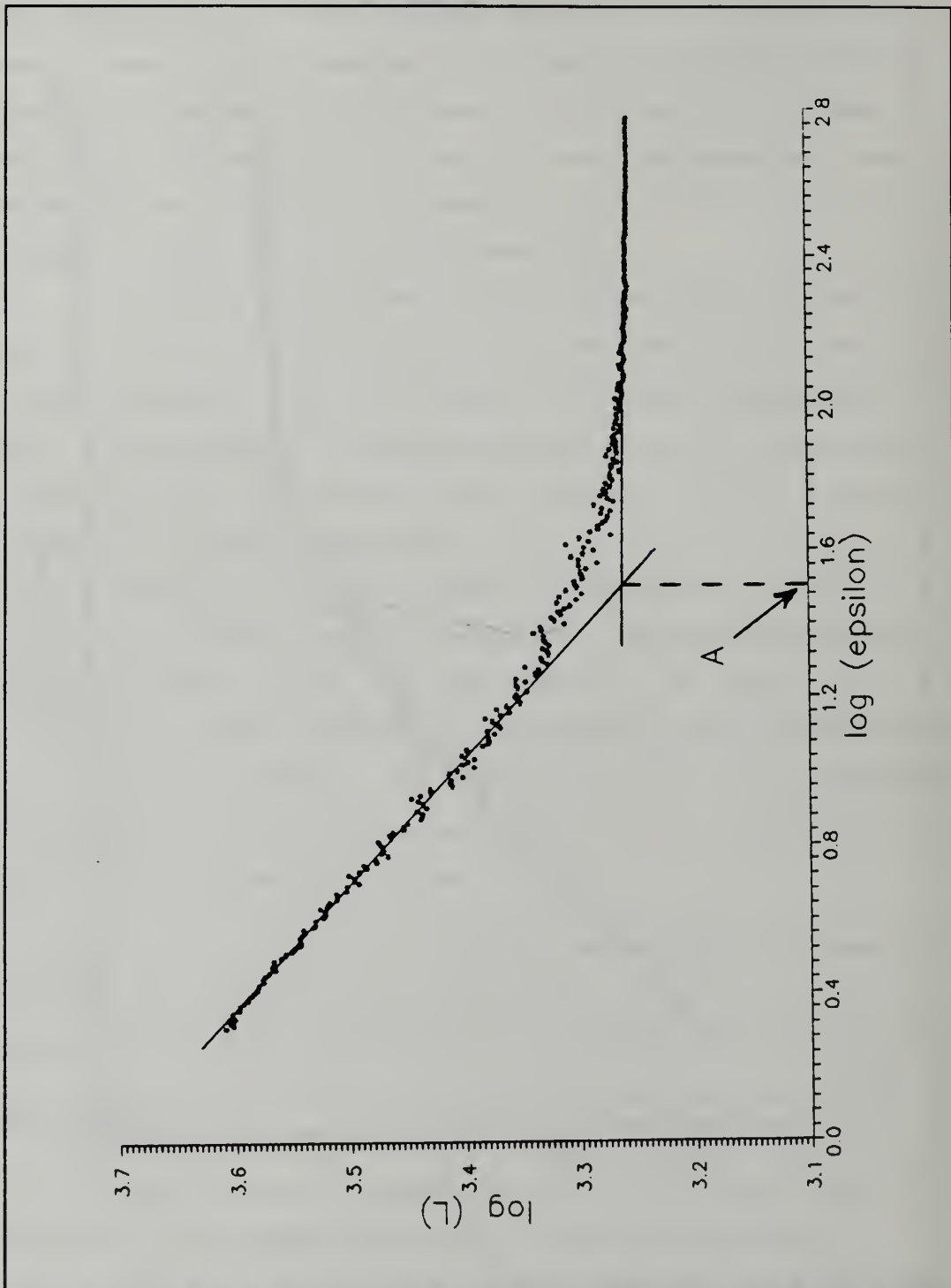Figure 4 – Typical log-log plot from self-similar algorithm (D_C) from the temperature time series.

Figure 5 – Determination of largest ε to use in calculating slope for D_C.

2. D_A Analysis.

The characteristics of D_A were explored by applying the algorithm of McHardy and Czerny (ibid) to the time series and making log-log plots of the length metric as a function of ε, the time resolution. This wasdone for the temperature and three velocity components, using sequential three minute windows for the entire four hours of data. Three minute windows were chosen, since what appeared to be a gravity wave in the data had a period of about 200 seconds, and the hope was to resolve it and perhaps catch its onset and demise. The minimum ε used was two data points (.2 sec) because the time series scales linearly for $\varepsilon < 1$, sincea straight line was used to connect data points. The maximum ε was set to the window size of 1800 data points for the first run. This allowed approximately three decades of dynamic range.

The first run showed for all windows that log $L(\varepsilon)$ vs. log ε had constant, non-zero slope for ε from 2 (.2 sec) to around 600 (1 min). For $\varepsilon > 600$, many of the plots no longer had constant slope. Thus, to calculate D_A, only log $\varepsilon \leq 2.75$ ($\varepsilon \approx 600$) was used, since this still provided a satisfactory 2.5 decades along the ordinate. As discussed earlier, an additional reason for only using $\varepsilon < 600$ is that for a single sinusoid, log $L(\varepsilon)$ vs. log ε shows nearly zero slope for ε less than a third of the wave period (Figure 2), whereas for $\varepsilon > 600$ the plot is nearly vertical. Since the wave in the data had a period of around 3 minutes, or 1800 data points, taking ε to be less than 600 data points assures that D_A will be calculated in the portion of the plot that is linear and nearly horizontal. Thus, unlike D_C, no subjective window by window cutoff of ε is needed to calculate D_A.

To get D_A for each window, again the simple linear regression from Beyer (ibid) was used to fit a line through the log-log plot.

3.   **Determination of Mean Turbulent Kinetic Energy (TKE).**

Mean turbulent kinetic energy is defined as $\frac{1}{2}(\sigma_u^2 + \sigma_v^2 + \sigma_w^2)$, where σ_u, σ_v, and σ_w are the respective standard deviations of u, v, and w. Stull (ibid) notes that it is customary to find the variances over a period of 30 minutes to one hour, because the apparent "spectral gap" occurs at about 1 hour, and allows a convenient separation between "large" scales and "small" scales. However, this procedure includes all variations as "turbulence"; so it would include gravity wave energy along with real turbulent energy.

For comparison, TKE and variances were calculated instead over the same three minute intervals as D_C and D_A. All other parameters such as bulk Richardson number or Brunt-Väisälä frequency were also calculated over three minute windows. It should be emphasized that this will not eliminate the problem of counting gravity wave kinetic energy as turbulent kinetic energy.

4.   **Bulk Richardson Number (R_B) Determination.**

Richardson number was evaluated for possible correlations with D_C or D_A. Ideally, the flux Richardson number, R_f, or the gradient Richardson number, R_i, should be used, since the interest is in the local stability at the sensor. Both R_f and R_i require that the local vertical gradient of the mean wind be known, but since the sensors were spaced 50 meters apart vertically, the local gradient was not available. Hence, the bulk Richardson number, R_B, was used.

$$R_B \equiv \frac{g\,\Delta\overline{\theta}_v\,\Delta z}{\overline{\theta}_v\,[(\Delta\overline{U})^2 + (\Delta\overline{V})^2]} \ ,$$

where Δ represents the quantity difference between the bottom and top of the layer. For the calculations the layer thickness, Δz, was 100 meters, with the layer centered on the level of interest.

The virtual potential temperature, θ_v, was assumed to be equal to the potential temperature, θ. Though Stull (ibid) emphasizes that θ_v

26

can differ from θ by up to 4°C, this will not seriously affect R_B for three reasons. First, $\partial\theta_v/\partial z$ will not differ much by substituting θ for θ_v; second, a 4°C difference in the denominator will not change R_B by more than 10 percent; and third, the absolute value of R_B is not important. R_B is only important as an indication of stability changes.

R_B was block averaged over three minute windows to correlate it with D_A and D_C over the same window length.

   5.   **Determination of Brunt-Väisälä Frequency (BVF).**

The BVF was chosen to measure static stability and, like R_B, possible correlations with D_C or D_A were tested. BVF is defined as

$$\text{BVF} = \sqrt{\frac{g}{\overline{\theta}_v}\frac{\partial \overline{\theta}_v}{\partial z}} \; .$$

As with R_B, the quantity $\partial\overline{\theta}_v/\partial z$ was approximated by $\Delta\overline{\theta}/\Delta z$; thus, it is not a local measure of static stability. θ was again assumed equivalent to θ_v because the interest was in changes in BVF with time, not actual values.

   6.   **Buoyancy Length (l_B).**

l_B is given in Stull (ibid) as the standard deviation of the vertical velocity divided by the Brunt-Väisälä frequency ($l_B = \sigma_w/\text{BVF}$), and is meant to be a measure of the dominant eddy scale.

IV. RESULTS AND DISCUSSION

A.   WAVE AND TURBULENCE PERIODS.

Figure 3 shows a time series of the temperature data taken from the resistance wire. Cursory inspection shows both "wave" and "turbulence" like episodes. Figure 6(a), taken over three minute windows (1800 data points), shows several distinct periods where the temperature variance, σ_T^2, peaks. The most pronounced peak occurs from windows 21 through 28, cotaneous with what appears to be a wave. Three other periods are cotaneous with what appear to be turbulent fluctuations during windows 45 - 47, 64 - 67, and 73 - 75. The other σ_T^2 peaks, such as window 62, were caused by a continuous temperature change across the window that does not seem associated with either a wave or turbulence. This is missing in the three minute σ_v^2 and σ_w^2 records also shown in Figures 6(b) and (c), but does appear in σ_u^2 (Figure 6(d)). Again, the σ_u^2, σ_v^2, and σ_w^2 records do not distinguish between wave-like and turbulence-like episodes; all appear as local maxima.

Since the variances peak during what appears to be a wave portion of the time series, this suggests that variance by itself cannot reliably indicate the presence of turbulence, and thus indicate the dispersion rate of scalars such as heat or aerosols.

B.   FRACTAL DIMENSION, D_A, OF THE TIME SERIES.

Fractal dimension, D_A, on three minute windows was readily attainable from the time series. Figure 7 shows a typical log $L(\varepsilon)$ versus log ε plotfor the temperature data. Most of the plots remained nearly linear for up to three decades on the ordinate, (from $\varepsilon = 2$ (.2 sec.) to 600 (60 sec.)), lending robustness to the measured value of D_A.

Figure 8 shows a plot of the three minute D_A values. D_A varies throughout, with the lowest values occurring during the wave episode in
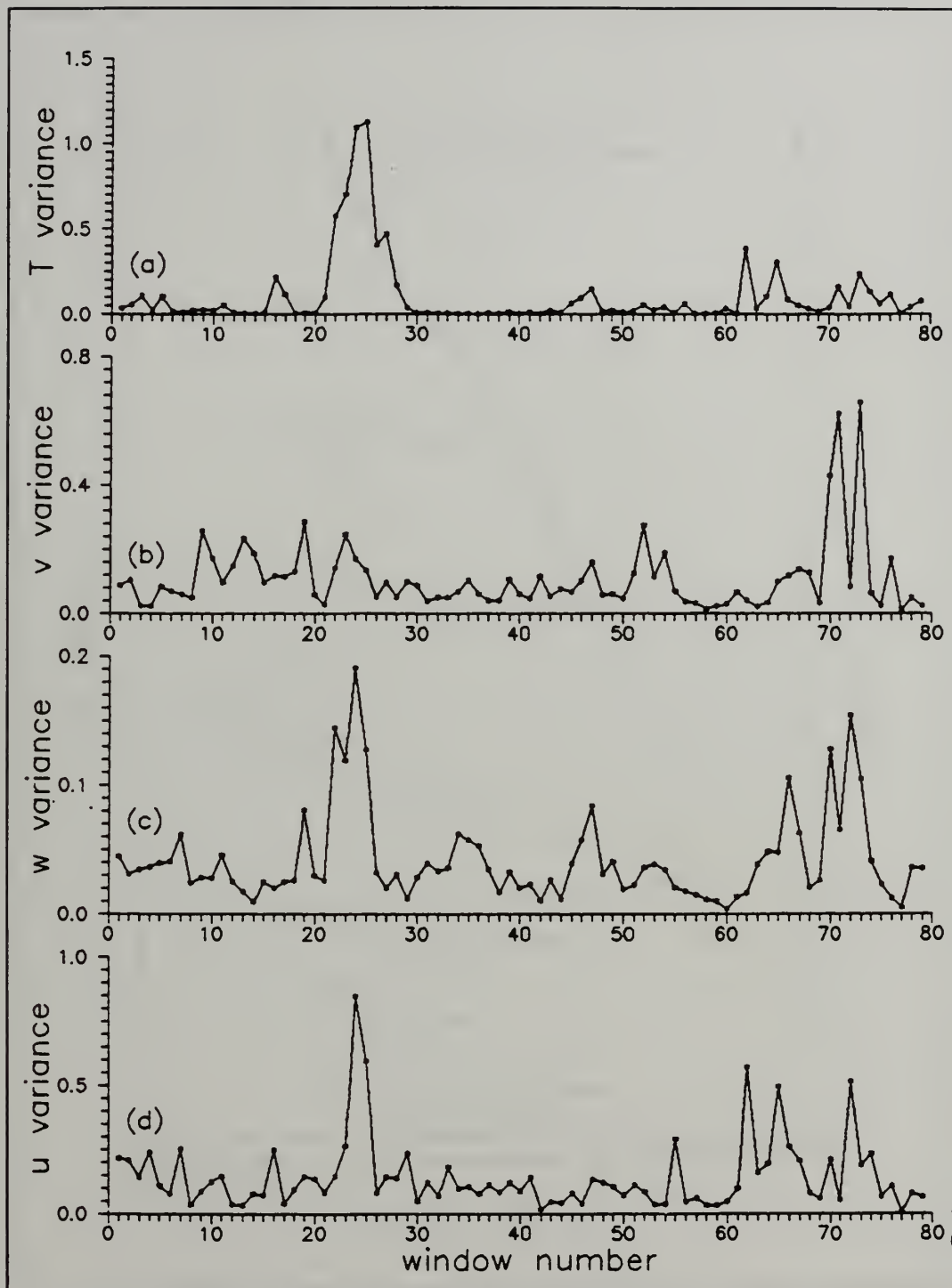
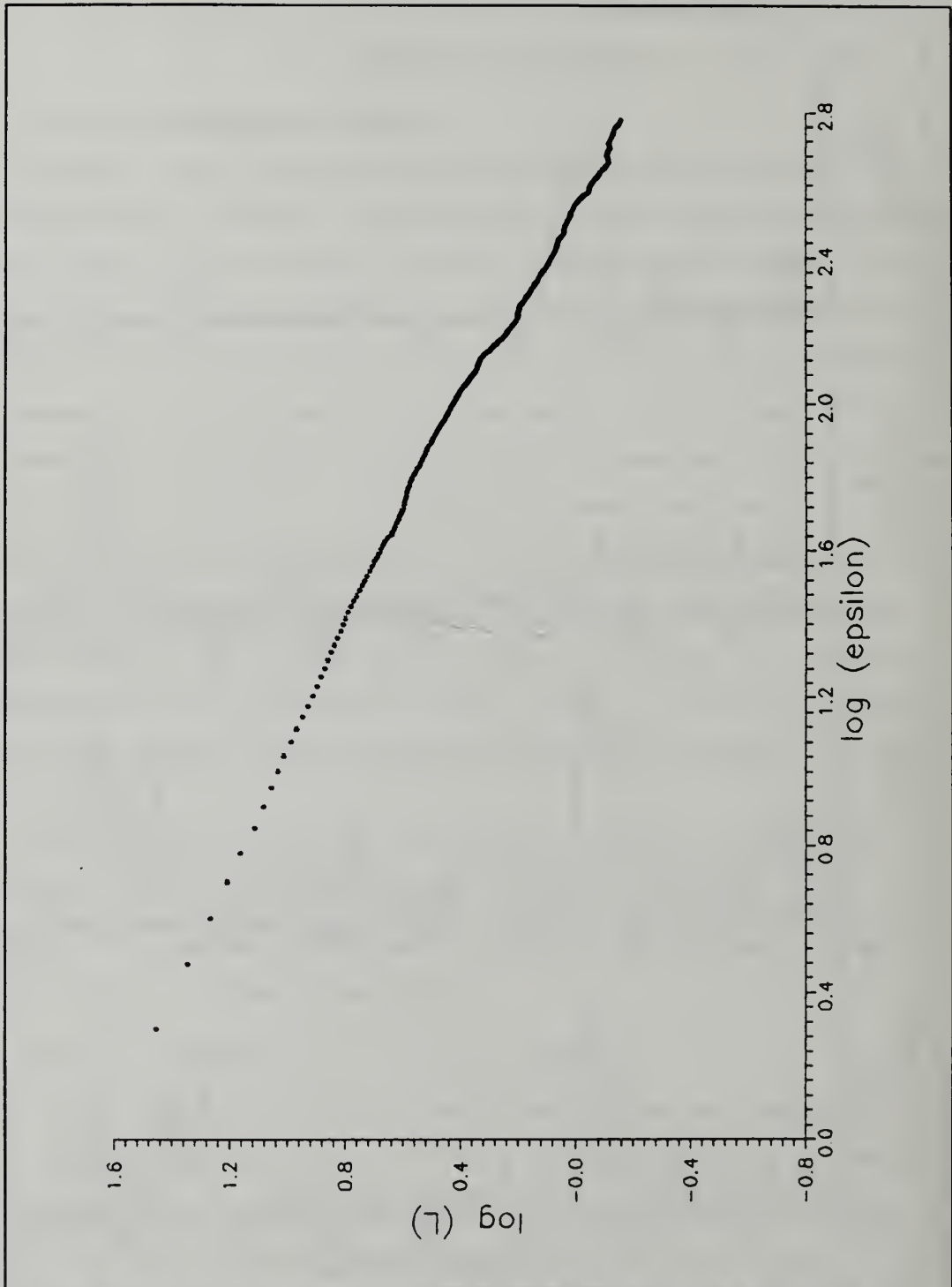Figure 6 - Variances of: (a) T; (b) v; (c) w; (d) u.

29

Figure 7 - Typical log-log plot from self-affine algorithm (D_A) from the temperature time series.
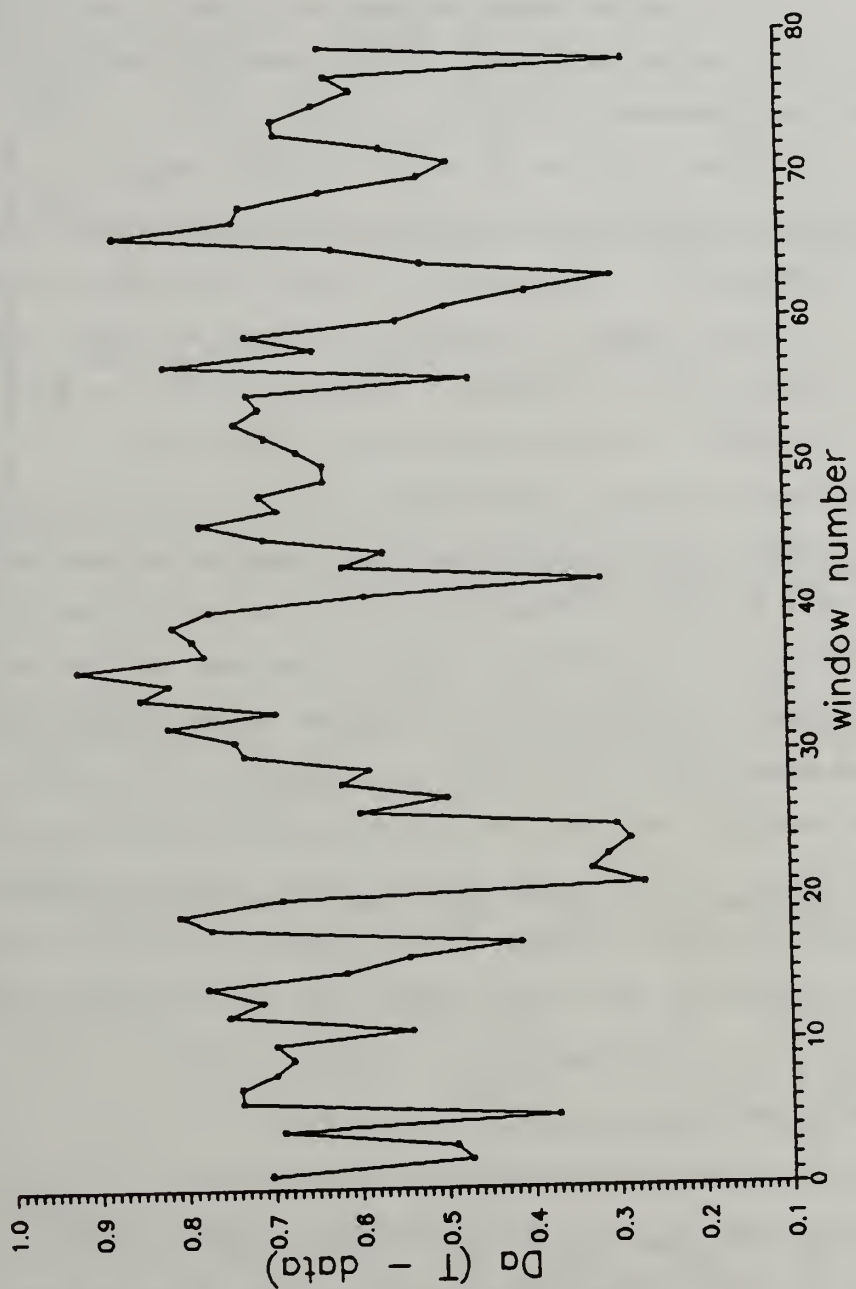
Figure 8 - D_A from temperature time series.

31

windows 21 through 28. There are three other distinct local minima occurring in windows 42, 63, and 78, which were associated with what appear to be low turbulence levels on the time series. Two of these minima occur just before maxima at windows 46 and 66 which are due to the "turbulent" episodes mentioned in the previous section. A possible rationale was discussed in section I.

This behavior of D_A is not confined to the temperature data. Figure 9 compares D_A from the temperature series with those from the three velocity components. The patterns of the D_A curves agree well, with the minima and maxima again occurring in or near the same windows on all plots. Scatter plots comparing D_A for one time series with another are given in Figure 10, and show good linear correlation. That the D_A for these different data sets agree closely lends confidence to this analysis.

The above results seem to discriminate between the wave and "turbulence" episodes, and agree well with the expectation that periods of wave activity or low turbulence should have lower D_A than more turbulent periods. However, the largest D_A at window 36 bears more scrutiny, since it is cotaneous with a relatively calm appearing, low variance portion of the time series. This may be because D_A, being self-affine, has a $1/\varepsilon$ scaling factor in the length metric, $L(\varepsilon)$, which gives more weight to variations at smaller scales. This region of the time series may be manifesting smaller scale turbulence. This topic was explored further in section I.

C. CONDITIONAL SAMPLING USING A D_A CUTOFF.

The above results point to the possible use of $D_A \approx 0.35$ from the temperature, or $D_A \approx 0.5$ from vertical velocity data as conditional sampling cut-off values to remove wave data from hot-wire and sonic anemometer recordings, while retaining most of the real turbulence. This would remove most of the inappropriate wave fluctuations from turbulence intensity and dispersion calculations. However, more data containing both
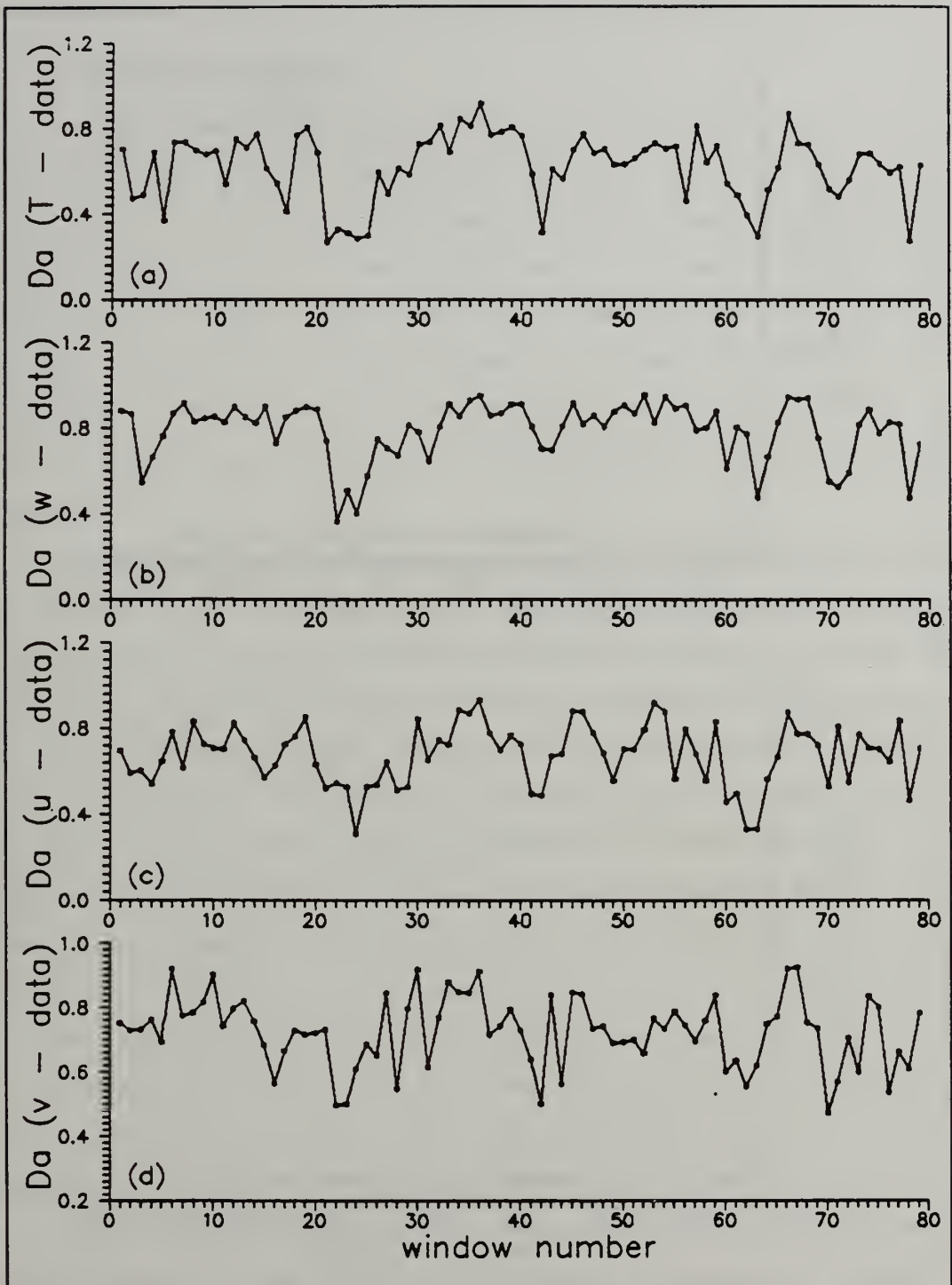
32

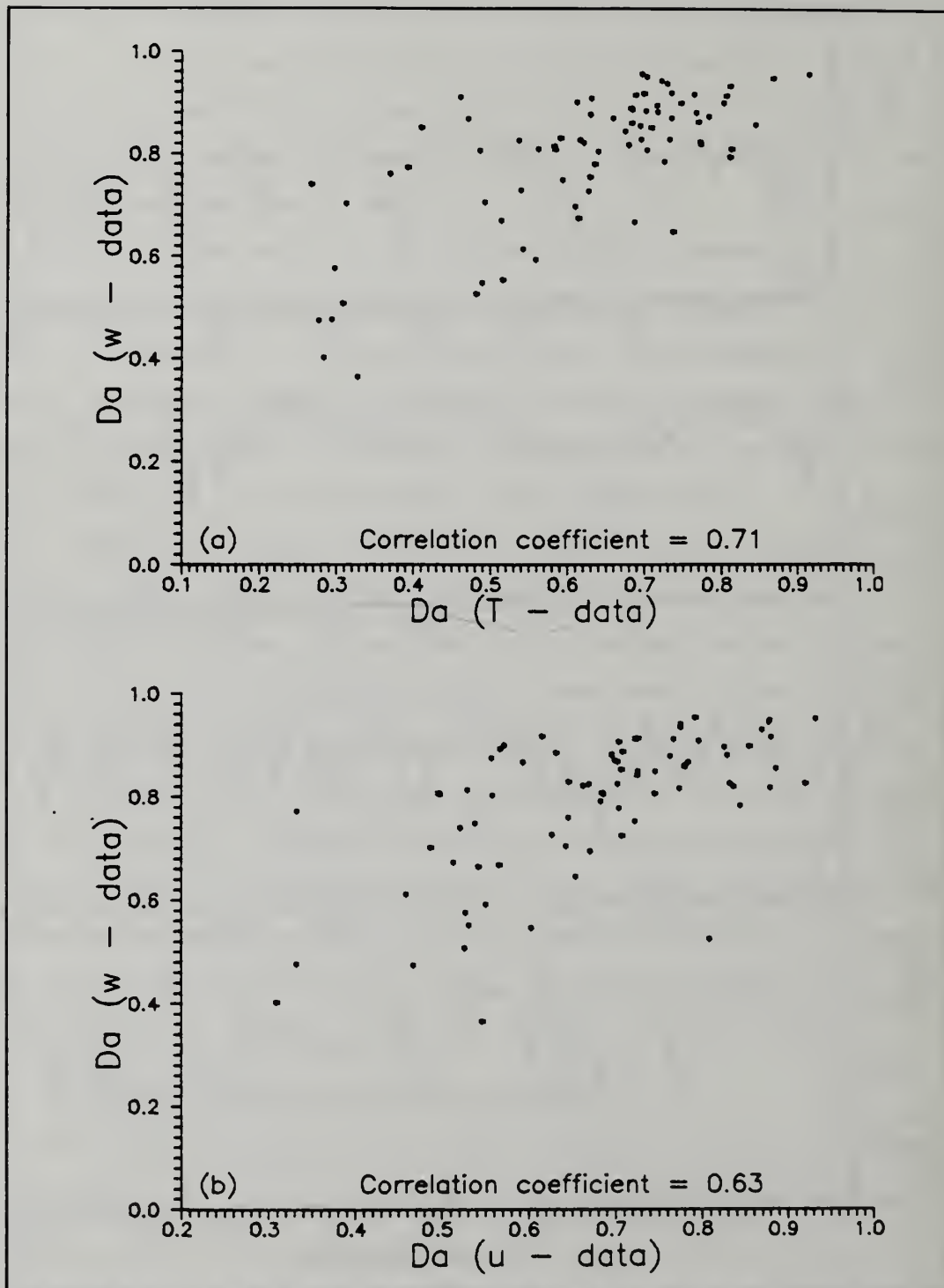Figure 9 - D_A from: (a) T; (b) w; (c) u; and (d) v time series.

Figure 10 - Scattergrams of D_A from: (a) T vs. w; (b) u vs. w.

waves and turbulence must be analyzed before being able to state this with confidence.

D. D_A AND BREAKING WAVES.

In the latter part of the "wave" period, all values of D_A calculated from the T, u, v, and w time series show jumps which are cotaneous with the advent of a gain in high frequency fluctuations in the T and w time series.   These may indicate "wave break", or a wave-turbulence energy transfer event. Again, the variances and TKE show the opposite behavior, falling precipitously.   This suggests that, unlike other purely local measures, D_A may be useful in determining wave break episodes.   Local minima in D_A of short duration are also seen prior to the three turbulence episodes.

A suggested turbulence generation mechanism (Gossard, ibid) explained in Chapter II, is repeated here.   This mechanism requires that local gradients of θ, u, and v increase steadily, together with decreasing turbulence.   The vertical shear eventually reaches an insupportable value of local Richardson number, leading to local Kelvin-Helmholtz instability and a rapid onset of fluctuations growing into turbulence.   Waves may augment the local shear, thereby instigating an instability, but this may also occur in the absence of waves.   The above observed local D_A minima, just prior to rapidly growing fluctuations for both the "wave break" and "turbulent" episodes, is consistent with this proposed mechanism. However, the local critical Richardson number hypothesis could not be tested readily with this data set, due to the minimum 50 meter vertical separation of the sensors.   The bulk Richardson number, R_B, which was measured, does plummet at what appears to be the time of "wave break", as well as prior to one of the "turbulence" episodes, but this does not occur prior to the other two turbulence periods.

E.   FRACTAL DIMENSION, D_C.

Since this form of fractal dimension is sensitive to the scaling of the y-axis of the time series, an arbitrary scaling of .1 second = 100°C was chosen. As expected, D_C behaved differently from D_A, rising dramatically during the wave episode, and falling immediately after. This same behavior was observed during the turbulent episodes; thus, D_C did not distinguish between the wave and turbulence. Moreover, the algorithm is long and ad hoc, with its assumed y-axis scaling and subjective cutoffs for calculating slopes of the log-log plots. Moreover, Mandelbrot (1985) warns that it is ill-suited for application to self-affine data such as used in this study. These disadvantages led to the sole use of D_A for subsequent analysis.

F.   FRACTAL DIMENSION AS CORRELATED WITH BULK MEASURES OF STABILITY.

Figures 11(a) and (b) show the temperature D_A compared with Brunt-Väisälä frequency (BVF). The BVF is highest during the wave episode when D_A is minimum. The three minima in D_A at windows 42, 63, and 78 occur when the BVF is at or near a local maximum, consistent with the fact that a higher BVF (more stable) will tend to dampen turbulence. Also significant is that most of the D_A maxima occur when the BVF is either decreasing or at a minimum, which indicates a less stable and more turbulent atmosphere. However, high values of BVF occurred during both wave-like and turbulence-like episodes, indicating little use in resolving the two. Figure 11(c) shows a scatter plot of temperature D_A versus BVF, which indicates a weak inverse correlation.

Figure 12 shows another weak, but positive, correlation between D_A and l_B, the buoyancy length scale. The correlation is highest during the "wave" episode, when l_B drops rapidly, simultaneous with a rapid drop in D_A. After the wave episode, D_A and l_B both rise.

The u and T variances and BVF show local maxima at window 62, while the u and w variances and l_B show local minima. The T time series shows
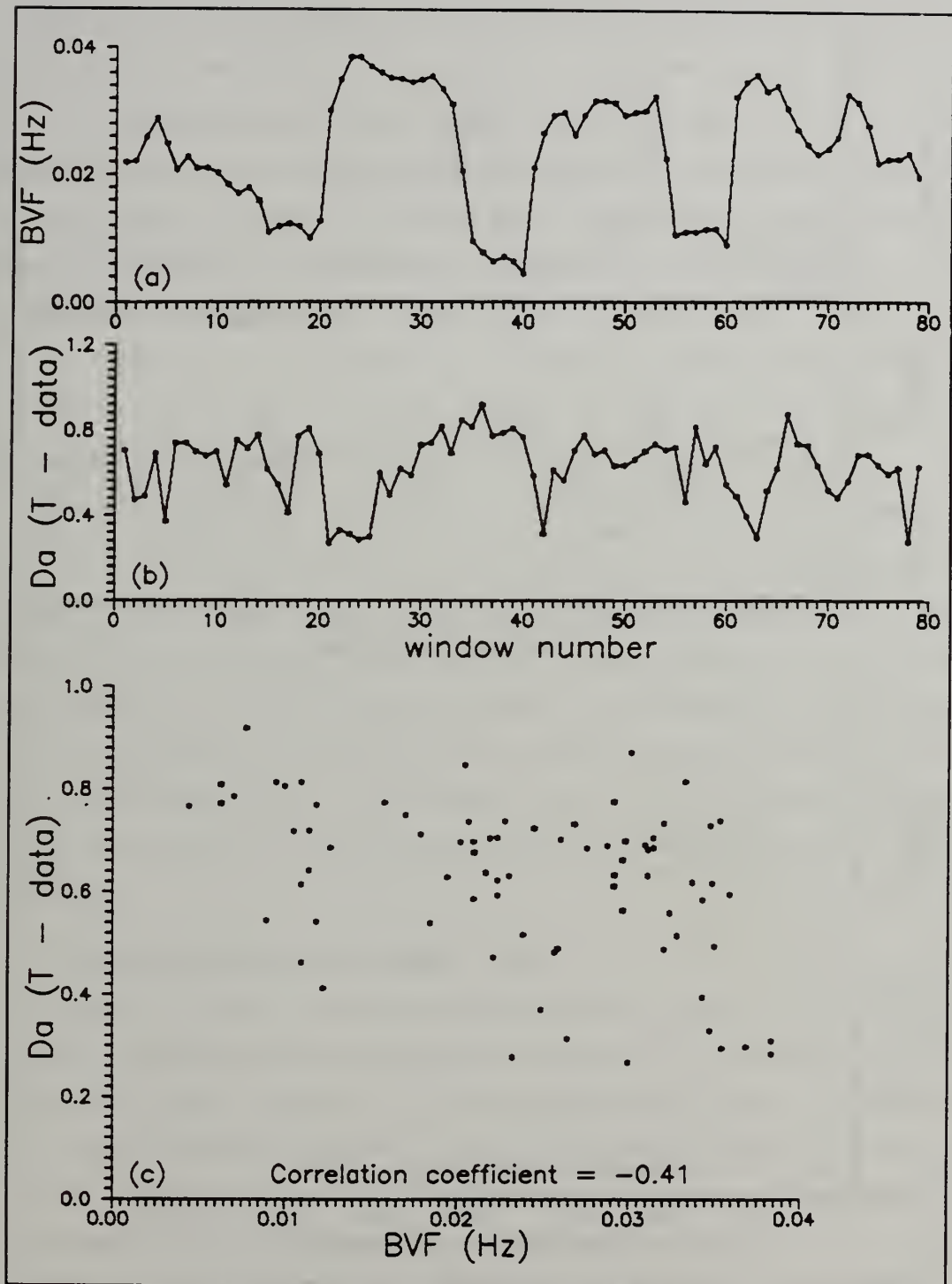
36

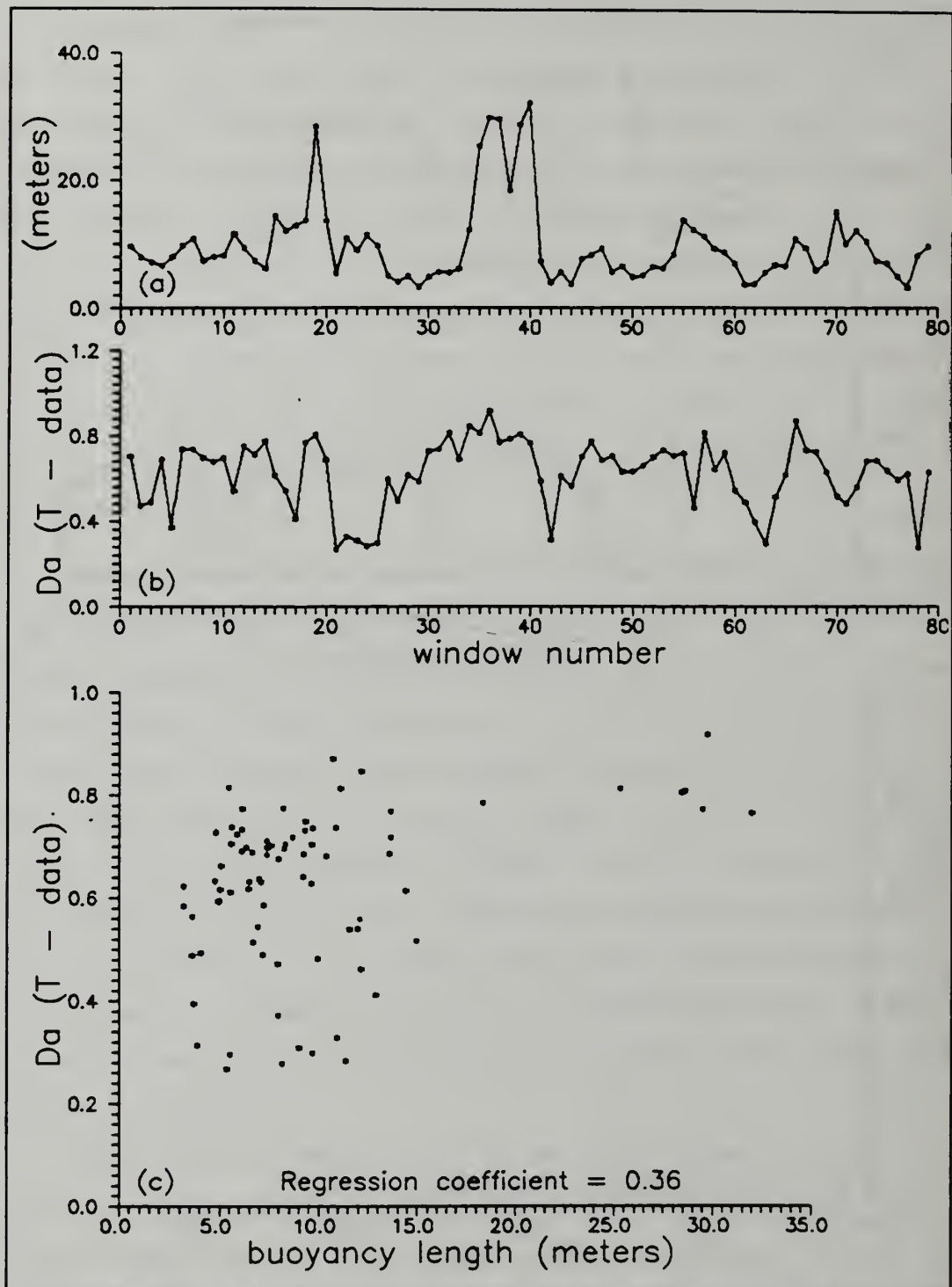Figure 11 - (a) BVF; (b) D_A from T time series; (c) D_A vs. BVF.

Figure 12 – (a) l_B; (b) D_A from T time series; (c) D_A vs. l_B.

an enduring but rapid fall in temperature. l_B does not seem to distinguish between wave-like and turbulence-like episodes. All such episodes show moderate l_B on the order of 8-12 meters. Since BVF is in the denominator of l_B, l_B peaks during windows 18-20, and 35-40 when BVF is low. This seems to occur when the temperature time series is relatively calm. Thus, large l_B does not seem to correlate with turbulence-like episodes, and l_B does not seem to be a good measure of dominant eddy scale, as has previously been suggested.

A comparison of D_A with R_B in Figure 13 shows little correlation between these quantities, except during the "wave" period when R_B rises dramatically, indicating an increase in stability.

High correlations between D_A and BVF, R_B, or l_B are not expected since D_A is a local measure, whereas the latter three are bulk measures which include measurements from widely vertically separated sensors. Correlations might have been higher if more local but still accurate measurements of $\Delta\theta$ and Δu were available. Unfortunately this capability is not now present on the BAO tower or other like facilities such as the RISØ Lamme-Fjord tower. In any event, none of the bulk measures seem to readily or consistently distinguish between wave-like and turbulence-like episodes.

G.   MEAN TURBULENT KINETIC ENERGY (TKE).

Figure 14 shows the mean turbulent kinetic energy over three minute windows. Like the variances themselves (Figure 6), the TKE shows a spike during the "wave" episode, and similar spikes are also displayed during the three "turbulent" episodes. Again, the results indicate that neither the TKE nor the component variances distinguish between waves and turbulence; both may have similar magnitudes.
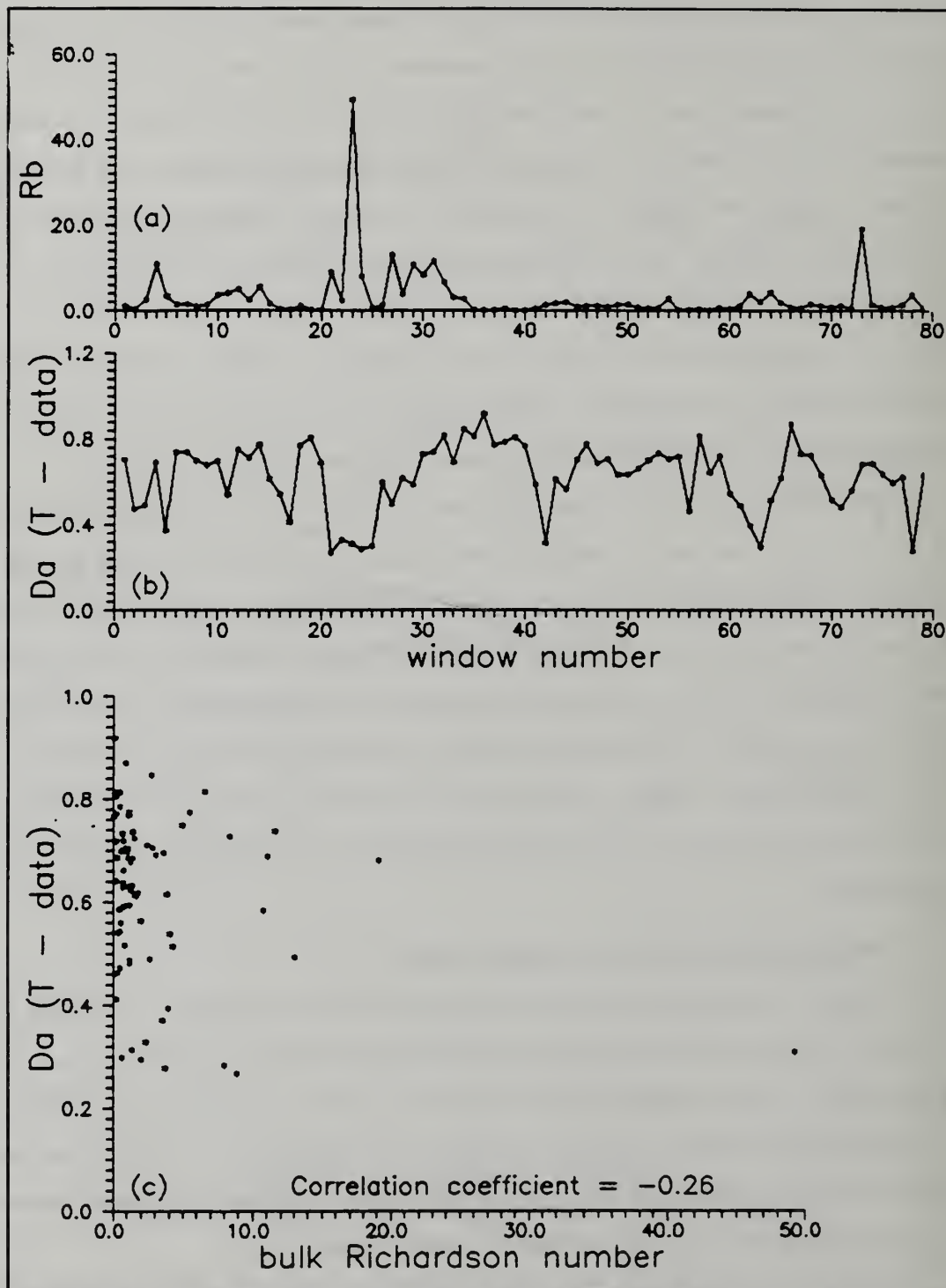
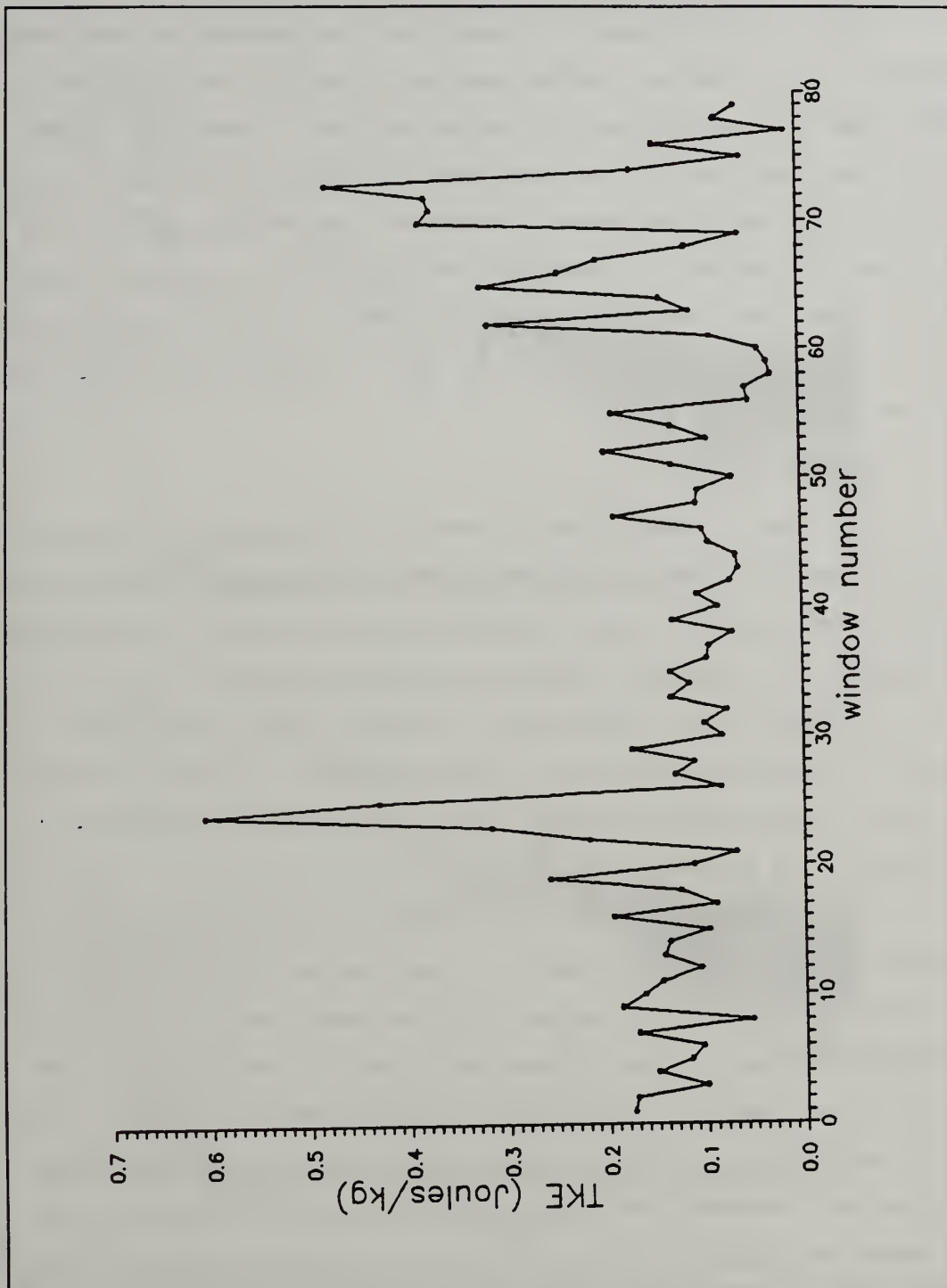Figure 13 - (a) R_B; (b) D_A from T time series; (c) D_A vs. R_B.

Figure 14 - Mean turbulent kinetic energy (TKE).

H. FAST FOURIER TRANSFORM (FFT) SPECTRA.

Figure 15 shows spectral density of the temperature data before and during the wave period. Before performing the FFT, the data were linearly detrended and tapered using a cosine squared, or Hanning, window. Even after such processing, the FFT spectral density plots are quite noisy, andshow only slight evidence of a spectral gap between the wave and higher frequency turbulent fluctuations during the wave episode. One would expect that the energy in components above 0.1 Hz would be heightened during these episodes. This is not reliably evident as shown in Figure 16.

I. ANOTHER LOOK AT D_A.

One possible reason why D_A seems to distinguish between waves and turbulence is that the factor $1/\varepsilon$ in the length metric weights the smaller scales more heavily, and in the stable boundary layer the turbulence is expected to be generally smaller scale than waves.

If this is true, then D_A may be simply a "scale separator", and its ability to separate waves from turbulence might be lost in a decreasingly stable, or convective boundary layer where turbulence scales may be as large as wave scales.

This could also explain the anomalous rise in D_A after the "wave" episode, described in section B, during a period of what appears to be low turbulence in the time series. On the other hand, the wave breaks in windows 25-28 may initially blend the potential temperatures across levels 3 to 5 (see Figure 17), resulting in high l_B and low BVF after window 35. This is consistent with the local maxima in the w and v variances around window 35. However, the large D_A maxima in window 35 of the u, v, w, and T traces may suggest continued turbulent blending, principally at smaller scales, even after the level 4 and 5 potential temperatures have become well-mixed.
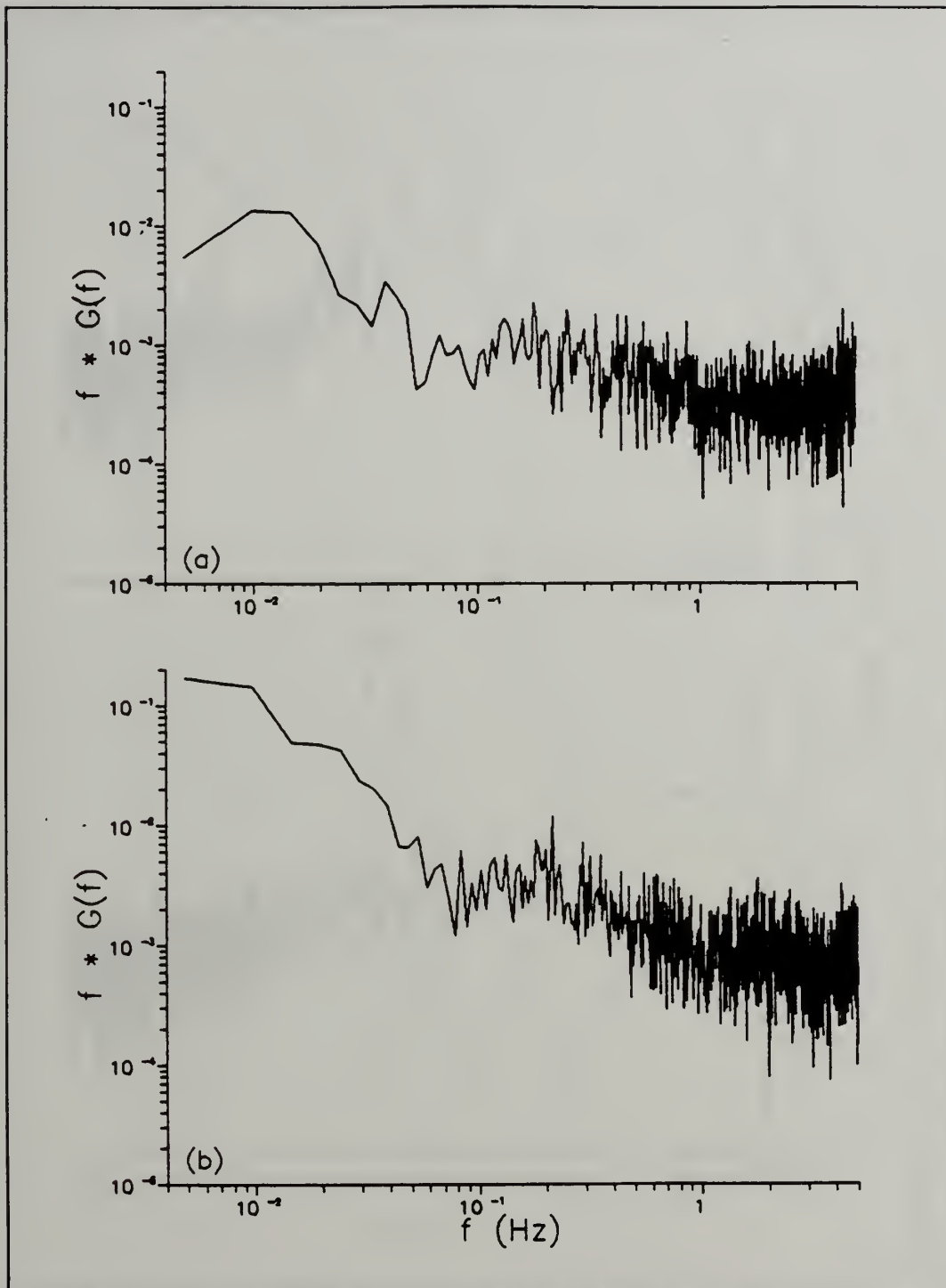
Figure 15 - FFT spectra from T time series: (a) before wave; and
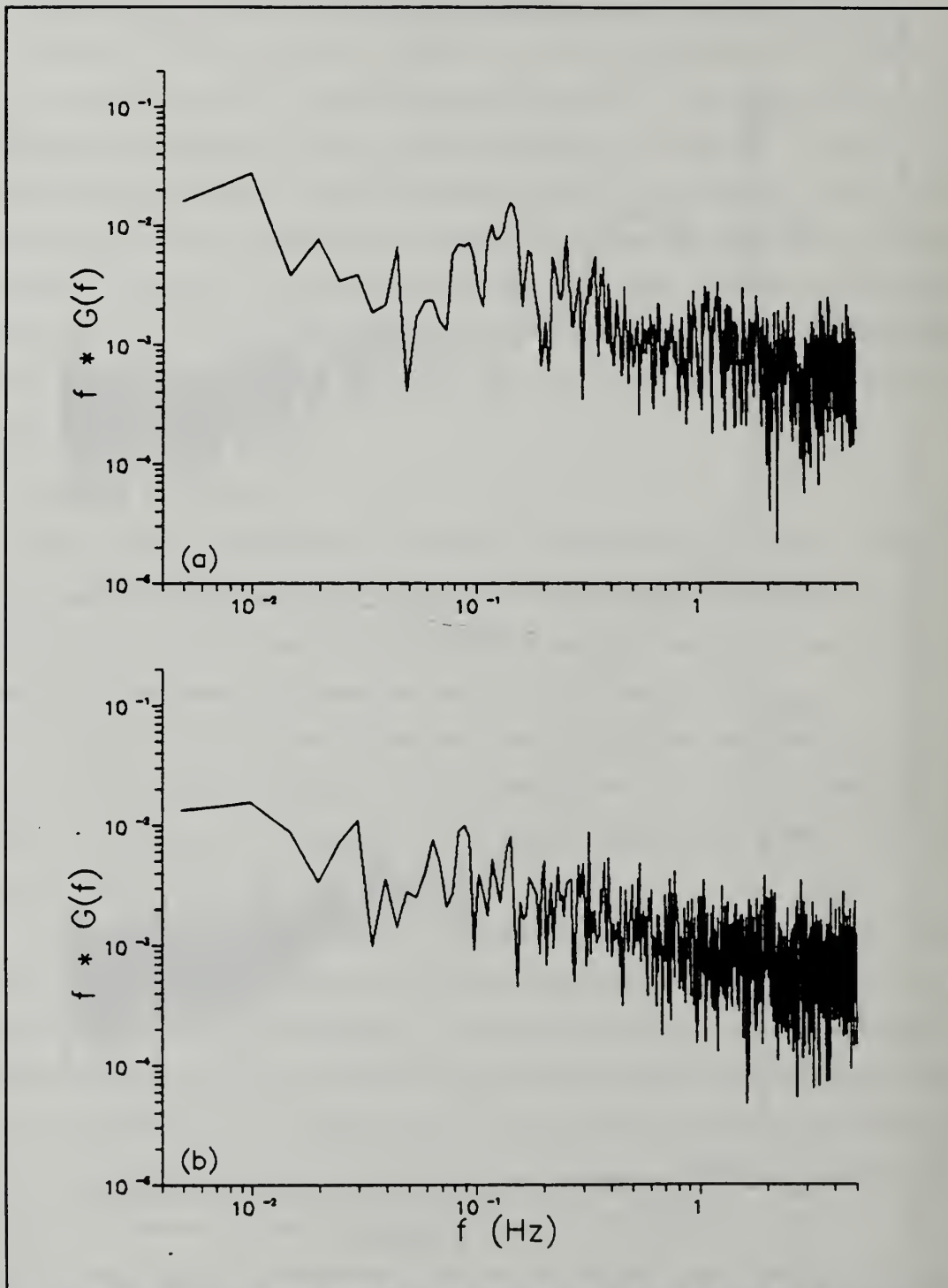(b) during wave.

Figure 16 - FFT spectra from T time series: (a) before third turbulent episode; and (b) during turbulence.
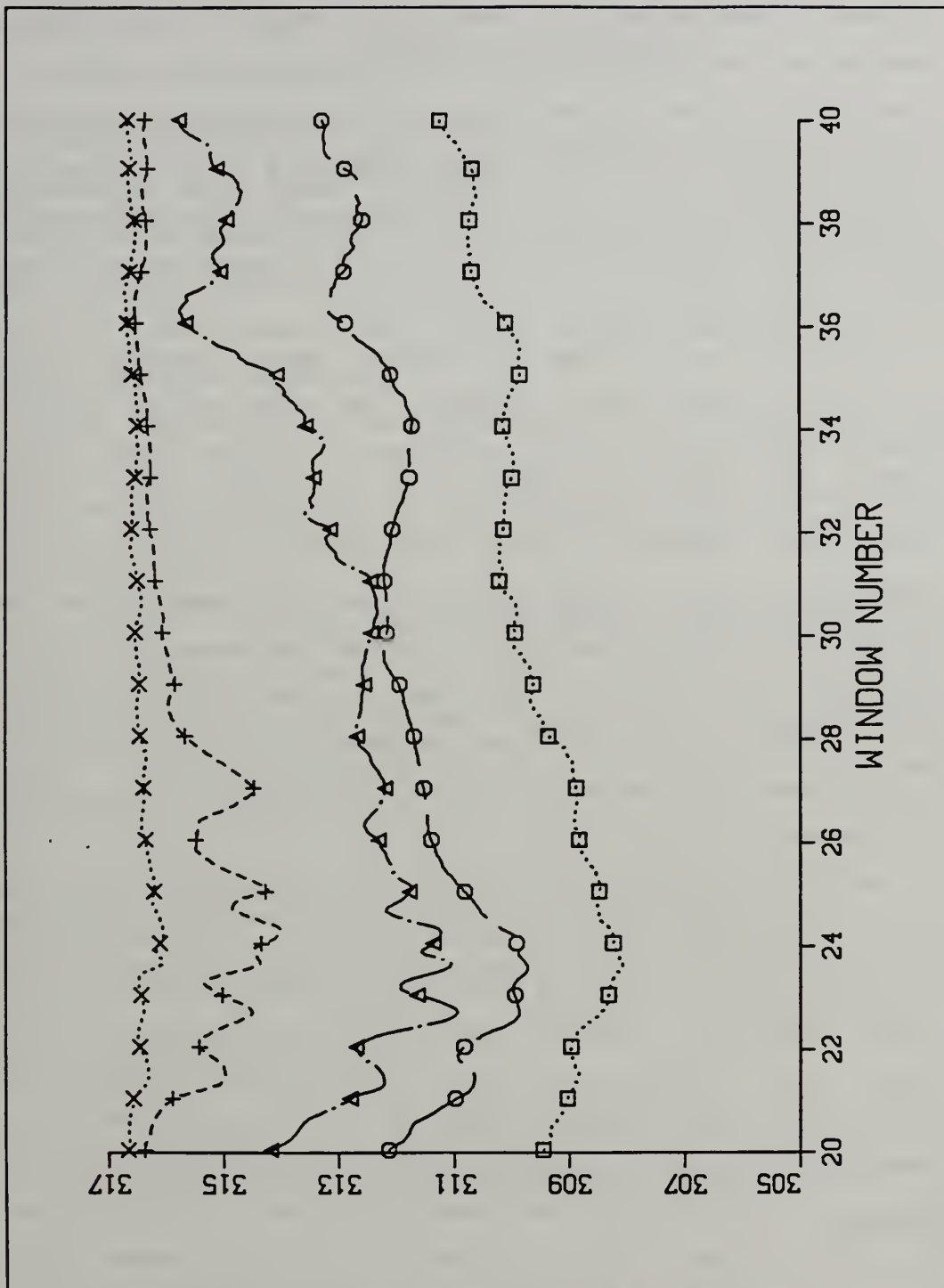
Figure 17 — θ profile (°K) during and after wave.
□ – 10 m; ○ – 22 m; Δ – 50 m; + – 100 m; x – 150 m

45

D_A for this perhaps smaller scale blending may be unduly accentuated by being normalized by $1/\varepsilon^n$, where n was assumed to equal unity. For inertial eddy cascade processes, n may indeed be less than unity. An n < 1 would tend to balance the effect on D_A from smaller scale turbulence. Future work might pursue this issue, attempting to find a theoretically justified value for n. This will also require a modification of the integrand in II.14 so that $L(\varepsilon)$ retains its proper units of amplitude only.

As a first guess, since the turbulence energy spectrum tends to have a $-\frac{5}{3}$ slope in the inertial subrange, one might expect the turbulence velocity spectrum to have a $-(\frac{5}{3})^{\frac{1}{2}}$ slope. In that case, perhaps the correct self-affinity factor for inertial subrange turbulence should be n = $(\frac{2}{3})^{\frac{1}{2}}$ = 0.82. However, the BAO data resolution is 0.1 seconds, which enters the dissipation range where the spectral energy slopes are much higher. To eliminate contributions from this range, the inner scale cutoff would have to be at longer times, thus narrowing the dynamic range over which D_A is computed. This may be possible for convective data, since a longer window must be used to capture fluctuations due to boundary layer scale eddies.

Another potential complication for such an analysis is that stability tends to compress the vertical extent of an eddy. Thus, inertial subrange turbulence may not have a $-\frac{5}{3}$ slope in the energy spectrum, as in self-similar turbulence. That is, there will be less energy in the larger scales. Mahrt and Gamage (1987) have studied vertical/horizontal velocity aspect ratios for structure functions as a function of stability. However, their stability categories were not well defined by R_i or other measures.

IV. SUMMARY AND CONCLUSIONS

Time series of T, u, v, and w from a stable atmospheric boundary layer were examined using fractal techniques. The time series were taken from a height of 100 meters on the mast at the Boulder Atmospheric Observatory (BAO) and were sampled at a rate of 10 Hz. The time series contained a period of what appeared to be a terrain induced gravity wave as well as several periods of turbulence.

Both self-similar fractal dimension, D_C, and self-affine fractal dimension, D_A, were used in the analysis. The latter was found to be superior. This is because time series are inherently self-affine, rather than self-similar.

D_A appears to easily distinguish between the wave and turbulent episodes, showing minima during wave episodes and maxima during turbulence. It was the only parameter studied that reliably distinguished the two. A conditional sampling cutoff of $D_A \approx 0.35$ from fast response temperature data is suggested as a possible wave indicator, though further study is needed before this can be stated with confidence. Since σ_w^2 peaks during both waves and turbulence, dividing D_A by σ_w^2 could aid in finding waves in the data by further enhancing the difference in D_A between waves and turbulence. Similarly, turbulent episodes could be further distinguished by multiplying D_A by σ_w^2.

The need to account for the presence of waves when calculating scalar dispersion in the atmosphere was discussed, and three currently used non-fractal methods for separating waves from turbulence data were described. D_A also shows promise as a means to resolve wave-turbulence energy transfers, or "wave break" events.

Correlations between D_A and various bulk measures of stability were investigated, with weak correlations (correlation coefficient ≤ .41) found with Brunt-Väisälä frequency (BVF) and buoyancy length (l_B), and little correlation with bulk Richardson number (R_B). The difficulty of trying to correlate a local measure, such as D_A, with bulk measures was discussed. These bulk measures were not useful discriminators of waves and turbulence.

Other possible parameters for distinguishing waves and turbulence were investigated. Turbulent kinetic energy (TKE) proved less than useful because wave energy must be included, unless removed through phase-averaging, which can only be applied to very ideal cases. Fast Fourier Transform spectral plots were somewhat useful, showing a weak spectral gap; however, their temporal resolution was poor, and the presence of a spectral gap is not guaranteed. The computational demands of FFT methods are also inherently much greater than in calculating D_A. Since D_A seems well-behaved, it may be computed by determining L only at the inner and outer time resolutions. Moreover, FFTs tend to treat finite wave trains, i.e., discontinuities quite poorly. D_A avoids this problem because it involves local Chapeau basis functions, rather than global transcendental or other basis functions. This makes D_A a potentially suitable analysis tool for turbulence intermittency and coherent structures.

Finally, the possibility that D_A acts as a "scale" discriminator rather than a wave/turbulence discriminator was discussed, and further investigation extending this form of analysis to convective data is suggested to explore this possibility.

An $n = (\frac{2}{3})^{\frac{1}{2}}$ self-affine scaling factor for ε is proposed as perhaps more suitable for turbulence, though this would require modification of the integrand in II.14 so that $L(\varepsilon)$ will not be a function of time. More data involving both waves and turbulence should be analyzed, using the

above techniques to verify these results and more narrowly specify cut-off values, etc.

Correlations between D_A and "wave-break" should be tested in more detail, perhaps with the Gossard (ibid) data set which involved vertical carriage traverses along the BAO tower, wherein local values of R_i were measured. Ultimately, one would like to establish D_A as a function of local stability, so that D_A turbulence cut-off values could be associated with critical R_i.

REFERENCES

Atlas, D., and J. I. Metcalf, 1970: The birth of "CAT" and microscale turbulence.,*J. Atmos. Sci.*,**27**,903-913.

Beyer, W. H., 1987: *CRC standard mathematical tables.*, CRC Press.

Carter, P. H., R. Cawley, A. L. Licht, and J. A. Yorke, 1986: in *Dimension and entropies in chaotic systems.*, edited by G. Mayer-Kress, Springer-Verlag.

Caughey, S. J., 1977: Boundary-layer turbulence spectra in stable conditions.*Bound.-Layer Meteor.*,**11**,3-14.

-----, and C. J. Readings, 1975: An observation of waves and turbulence in the Earth's boundary layer.*Bound.-Layer Meteor.*,**9**,279-296.

Finnigan, J. J., 1988: Kinetic energy transfer between internal gravity waves and turbulence.*J. Atmos. Sci.*,**45**,486-505.

Gossard, E. E., J. E. Gaynor, R. J. Zamora, and W. D. Neff, 1985: Finestructure of elevated stable layers observed by sounder and in situ tower sensors.*J. Atmos. Sci.*,**42**,2156-2169.

Grebogi, C., E. Ott, and J. Yorke, 1987: Chaos, strange attractors, and fractal basin boundaries in nonlinear dynamics.*Science.*,**238**, 632-638.

Hines, C. O., 1988: Generation of turbulence by atmospheric gravity waves.*J. Atmos. Sci.*,**45**,1269-1278.

Hunt, J. C. R., 1980: in *Workshop on the Planetary Boundary Layer.*, edited by J. C. Wyngaard, Amer. Meteor. Soc.

Kaimal, J. C., and J. E. Gaynor, 1983: The Boulder Atmospheric Observatory.*J. Appl. Meteor.*,**22**,863-880.

Mahrt, L., and N. Gamage, 1987: Observations of turbulence in stratified flow.,*J. Atmos. Sci.*,**44**,1106-1121.

Mandelbrot, B. B., 1977: *The fractal geometry of nature*, W. H. Freeman and Company.

-----, 1985: Self-affine fractals and fractal dimension. *Physica Scripta.*,**32**,257-260.

McHardy, I., and B. Czerny, 1987: Fractal X-ray time variability and spectral invariance of the Seyfert galaxy NGC5506.*Nature,***325**, 696-698.

Moon, F. C., 1987: *Chaotic vibrations*, John Wiley and Sons.

Nai-Ping, L., 1983: Wave and turbulence structure in a disturbed nocturnal inversion.,*Bound.-Layer Meteor.*,**26**,141-155.

Packard, N. H., J. P. Crutchfield, J. D. Farmer, and R. S. Shaw, 1980: Geometry from a time series.,*Phys. Rev. Lett.*,**45**,712-716.

Pawelzik, K., and H. G. Schuster, 1987: Generalized dimensions and entropies from a measured time series.,*Phys. Rev. A*,35,481-484.

Presad, R. R., and K. R. Sreenivasan, 1990: The measurement and interpretation of fractal dimensions of the scalar interface in turbulent flows., *Phys. Fluids A,***2**,792-807.

Richardson, L. F., 1922: *Weather prediction by numerical process.*, Cambridge Univ. Press.

Schertzer, D., and S. Lovejoy, 1984: in *Turbulence and chaotic phenomena in fluids.*, edited by T. Tatsumi, Elsevier Science Publishers B.V.

Sreenivasan, K. R., and C. Meneveau, 1986: The fractal facets of turbulence., *J. Fluid Mech.,***173**,357-386.

Stull, R. B., 1988: *An Introduction to Boundary Layer Meteorology*, Kluwar Academic Publishers.

INITIAL DISTRIBUTION LIST

1. Defense Technical Information Center   2
    Cameron Station
    Alexandria, VA 22304-6145

2. Library, Code 52   2
    Naval Postgraduate School
    Monterey, CA 93943-5000

3. Chairman (Code OC/Co)   1
    Department of Oceanography
    Naval Postgraduate School
    Monterey, CA 93943-5000

4. Chairman (Code MR/Hy)   1
    Department of Meteorology
    Naval Postgraduate School
    Monterey, CA 93943-5000

5. Ray Kamada (Code PH/Kd)   5
    Department of Physics
    Naval Postgraduate School
    Monterey, CA 93943-5000

6. Alex DeCaria   1
    825 E. Adams st.
    Layton, UT 84041

7. Ken Davidson (Code MR/Ds)   1
    Department of Meteorology
    Naval Postgraduate School
    Monterey, CA 93943-5000

8. Teddy Holt (Code MR/Ht)   1
    Department of Meteorology
    Naval Postgraduate School
    Monterey, CA 93943-5000

9. Bart Lundblad   1
    Aerospace Corporation
    Box 92957
    Los Angeles, CA 90009